

**Silk Implants for Localized Small Molecule  
Drug Delivery to Treat Traumatic Brain Injury**

A thesis submitted by

Varuna Rao

In partial fulfillment of the requirements for the degree of

*Master of Science*

in

*Biomedical Engineering*

**Tufts University**

May 2015

Advisor: David L. Kaplan, PhD

## **Abstract**

Traumatic brain injury (TBI) is the leading cause of death and disability worldwide. Resulting from blunt or penetrating forces to the head, TBI can affect any population of individuals. Following primary injury, or the initial mechanical insult, brain tissue undergoes secondary injury, notably necroptosis, or controlled tissue death. Administration of necroptosis inhibitors and other small molecules to alter the signaling cascade of tissue death has the potential to minimize the harmful short-term and long-term effects of secondary injury. Unfortunately, pharmaceuticals designed to target the brain have one major obstacle that medications to other sites of the body do not encounter - the blood barrier (BBB), a highly selective semi-permeable endothelial cell capillary network that protects the brain from toxic substances. The few drugs that successfully cross the BBB are only able to do so after reaching high systemic concentrations, adversely affecting the rest of the body. Invasive approaches by means of drug-eluting biodegradable polymer implants show greater potential for localized delivery. Among the most successful natural polymers is silk fibroin which boasts several qualities such as biocompatibility, biodegradability, and extraordinary tunability of chemical and mechanical properties, making it a very useful biomaterial for controlled local release of drugs to the brain for the treatment of TBI. In this research, two silk-based implants, thin silk films and silk-HRP hydrogels, were tested for their ability to consistently deliver small molecules to the brain and subsequently prevent cell and tissue death following a controlled cortical impact mouse model.

## **Acknowledgements**

The progress I have made on this project within the last two years would not have been made possible without the help of numerous people. First, I would like thank the person who provided me with this opportunity, Dr. David Kaplan, for his guidance, support and encouragement. As a professor and advisor, he has taught me the value of creativity and how to think outside-the-box in a research setting both of which have prepared me for my next steps as a working engineer. It has been an honor to be a part of his extremely diverse lab from whom I have learned so much.

Second, I would like to thank Dr. Michael Whalen for the opportunity to utilize his resources and conduct animal work. As a mentor, his time was invaluable and his clinical feedback contributed immensely to my education. It was a pleasure to work alongside him and be a part of his lab.

I would also like to extend my thanks to the members of the Whalen lab at Massachusetts General Hospital, Julie Golinski, Joon Chung and Jens Bak Sommer, all of whom trained me on mice work and assisted during numerous surgeries. My time with them was extremely enjoyable and I am grateful for the relationships we built.

Over at Tufts, I am very thankful for the countless people who made this experience possible. In particular, those at 200 Boston: Rod Jose, Joe Brown,

Jeannine Coburn, Katherine Polido, Maria Rodriguez, Dan Smoot and Annie Golding. They were always there to answer my questions and made coming to lab very enjoyable. Additionally, I would like to thank Min Tang-Schomer for introducing me to the project, and Ben Partlow, Maggie Wang and Jimmie White for their advice and help in the lab.

Last but not least, I would like to thank the several people who I did not see at either Tufts or MGH. I will forever be grateful to my family and friends for their endless love, support, motivation and encouragement during these last two years.

# Table of Contents

<b>Abstract.....</b>	<b>ii</b>
<b>Acknowledgements .....</b>	<b>iii</b>
<b>Table of Contents.....</b>	<b>v</b>
<b>List of Tables and Figures.....</b>	<b>vii</b>
<b>1. Introduction.....</b>	<b>2</b>
1.1 Significance.....	2
1.2 Specific Aims .....	4
<b>2. Background .....</b>	<b>6</b>
2.1 Traumatic brain injury .....	6
2.2 Primary injury .....	7
2.3 Secondary injury .....	8
2.4 TBI management with neuroimaging and .....	11
non-pharmaceutical therapies .....	11
2.5 Neuropharmaceutical therapy .....	14
2.6 Sites for therapeutic intervention .....	17
2.7 Challenges from translating between preclinical and .....	21
clinical studies.....	21
2.7.1 Common animal models for TBI .....	23
2.8 Silk implants for localized drug delivery .....	24
2.8.1 Thin silk films .....	28
2.8.2 Silk-HRP hydrogels .....	29
<b>3. Materials and Methods .....</b>	<b>30</b>
3.1 Silk fibroin extraction.....	30
3.2 Polydimethylsiloxane (PDMS) molds.....	30
3.3 Casting films .....	31
3.4 Enzymatically cross-linked hydrogels.....	33
3.4.1 In vitro release.....	33
3.5 In vivo subjects.....	34

3.6 Surgical implantation .....	34
3.7 Controlled cortical impact (CCI) .....	36
3.8 Sample preparation .....	37
<b>4. Thin Silk Films .....</b>	<b>38</b>
4.1 In vivo results .....	38
4.1.1 Single film implants .....	38
4.1.2 Dual film implants .....	40
4.1.3 Multiple dye-loaded film implants with adhesive .....	42
4.1.4 Transcortical transfer of dye from thin silk film implants .....	44
4.1.5 Small molecule delivery .....	49
4.2 Discussion.....	52
<b>5. Silk-HRP Hydrogels .....</b>	<b>57</b>
5.1 In vitro results .....	57
5.1.1 Hydrogel release .....	58
5.2 In vivo results .....	59
5.2.1 Silk-HRP hydrogel implants .....	59
5.2.2 Transcortical transfer of dye from silk-HRP hydrogels.....	61
5.2.3 Small molecule delivery .....	63
5.3 Discussion.....	65
<b>6. Conclusion .....</b>	<b>68</b>
6.1 Future Directions .....	69
6.1.1 Quantify in vitro release of small molecule drugs .....	69
6.1.2 Quantify in vivo release of small molecule drugs .....	71
6.1.3 Determine effect of delivery pre- and post-injury .....	72
6.1.4 Determine effect of large molecule drug delivery .....	73
<b>Bibliography .....</b>	<b>75</b>

## List of Tables and Figures

<i>Figure/Table</i>	<i>Title</i>	<i>Page</i>
<i>Table 1</i>	Small molecules for delivery via silk implants	4
<i>Figure 1</i>	Secondary injury signaling cascade initiated by primary brain injury and leading to cell and tissue death [16]	7
<i>Table 2</i>	Major markers of TBI and their significance	8
<i>Figure 2</i>	Overview of transport routes through the blood brain barrier via endogenous pathways [28]	14
<i>Figure 3</i>	Secondary injury signaling cascade labeled with potential sites for therapeutic intervention [16]	17
<i>Table 3</i>	Current neuropharmaceuticals and sites for therapeutic intervention	18
<i>Figure 4</i>	Silk films (4mm in diameter) loaded with Evans Blue dye drying on PDMS molds	31
<i>Figure 5</i>	Desiccator arranged to water-anneal silk films with a vacuum pressure of 20mmHg	31
<i>Figure 6</i>	Thin silk film implantation	34
<i>Figure 7</i>	Silk-HRP hydrogel implantation	35
<i>Figure 8</i>	Apparatus for controlled cortical impact. High air pressure is applied to a piston initiating impact direction onto the dura [34]	36

<b><i>Figure/Table</i></b>	<b><i>Title</i></b>	<b><i>Page</i></b>
<i>Figure 9</i>	Dye transfer from single film implantations of 2% w/v thin silk films water-annealed for 1, 3, 4 and 5 hours	38
<i>Figure 10</i>	Dye transfer from single film implantations of 5% w/v thin silk films water-annealed for 5 hours	39
<i>Figure 11</i>	Dye transfer from dual film implantations of 2% w/v thin silk films water-annealed for 1, 2, 4 and 5 hours	40
<i>Figure 12</i>	Dye transfer from dual film implantations of 5% w/v thin silk films water-annealed for 1 and 5 hours	41
<i>Figure 13</i>	Dye transfer from layering 5% w/v thin silk films water-annealed for 1 hour with application of adhesive on bone flap	42
<i>Figure 14</i>	Consistent dye transfer from two dye-loaded films (5% w/v silk, water-annealed for 1 hour) with the use of an adhesive on the bone flap	43
<i>Figure 15</i>	Schematic of film placement (left hemisphere) from coronal view which correlates to transcortical transfer images	44
<i>Figure 16</i>	Transcortical transfer of dye from single film implantations	44
<i>Figure 17</i>	Transcortical transfer of dye from dual film implantations	45
<i>Figure 18</i>	Transcortical transfer of dye from layering 5% w/v thin silk films water-annealed for 1 hour with application of adhesive on bone flap	47
<i>Figure 19</i>	Consistent transcortical transfer of dye from two dye-loaded films with application of adhesive on bone flap	48



<i><b>Figure/Table</b></i>	<i><b>Title</b></i>	<i><b>Page</b></i>
<i>Figure 20</i>	Sections with increased doses of propidium iodide (PI)	49
<i>Figure 21</i>	Sections from films loaded with PI and MK801	50
<i>Figure 22</i>	Intact post-implantation films loaded with PI	55
<i>Figure 23</i>	PI delivery via CSF to the choroid plexus	56
<i>Figure 24</i>	Dye release from hydrogels with different heights	57
<i>Figure 25</i>	Evans Blue dye release from hydrogels of different heights over 24 hours	57
<i>Figure 26</i>	Dye transfer from hydrogel implants of different heights	59
<i>Figure 27</i>	Transcortical transfer of dye from hydrogel implants of different heights	61
<i>Figure 28</i>	Sections from PI, GSH and dye delivery	62
<i>Figure 29</i>	Sections from GSH and dye delivery with intraperitoneal injection of PI	63
<i>Figure 30</i>	Intact post-implantation hydrogels	66

Silk Implants for Localized Small Molecule  
Drug Delivery to Treat Traumatic Brain Injury

# **1. Introduction**

## **1.1 Significance**

Traumatic brain injury (TBI) is a leading cause of death and disability worldwide accounting for approximately 2.2 million emergency department visits, 280,000 hospitalizations, and 50,000 deaths in one year in the United States alone, according to the Center for Disease Control and Prevention [1]. Additionally, recent data has found that of all injury-related deaths in the US, nearly one-third have at least one diagnosis of TBI [2]. Unfortunately, TBI incidence rates in developing countries are even higher with the World Health Organization predicting TBI to surpass many other diseases as the main cause of death and disability by the year 2030 [2]. While the most effected populations include children, young adults, and the elderly, TBI remains highly heterogeneous in terms of etiology, severity, and outcome making it difficult to diagnose and treat [3]. TBI can generally be classified as mild, moderate or severe with the most common being mild TBI (mTBI). Sometimes referred to as a concussion, mTBI cases often go unnoticed because many people do not seek medical attention [4]. Symptoms can persist for one year following injury or even lead to lifelong disability [2].

Another significant motivation for TBI research is its implications on several other neurodegenerative diseases namely Alzheimer's disease (AD), Parkinson's disease (PD), Amyotrophic Lateral Sclerosis (ALS), and chronic traumatic encephalopathy (CTE) [5]. Because TBI is difficult to diagnose, the secondary

injury mechanisms go unnoticed for long periods of time. However, they often appear slowly as one of these progressive diseases. Furthermore, as a large population grows to be over the age of 60 in the next decade, many are expected to be the victim of a neurodegenerative disease [5]. Thus, it is crucial to better understand potential risk factors for these such as those found in the delayed effects of TBI. Currently, it is known that while researching neurodegenerative diseases separately that they share similar biochemical signaling cascades that are also found in TBI and linking the two will benefit both fields of research [5]. The strongest evidence that exists between a neurodegenerative disease and TBI is with AD. Although results are conflicting, patients are 60% more likely to develop AD following TBI when compared to other diseases. Moreover, research has also indicated that previous cases of head trauma accelerate the onset of AD [6]. Both share similar pathologic features as well such as neuronal loss, and synaptic dysfunction and plaque deposition supporting a likely connection between the two [6]. The second most common neurodegenerative disease is PD. Head trauma was first linked to PD as a potential risk factor with boxers as they receive multiple hits to the head. Again, research continues to be conflicting with approximately half of studies reporting a relationship between PD and TBI. However, like AD, PD and TBI share similar pathologic features [5]. Unfortunately, little is known of the link between ALS and CTE with TBI other than that a vague relationship exists from observing athletes. Studies have shown that athletes of certain sports, soccer, football and boxing, have a significantly higher chance of developing these neurodegenerative diseases [7]. CTE is also

difficult to diagnose and is often mistaken for AD, PD or ALS, and thus a consistent link between CTE and TBI is elusive. However, both ALS and CTE again share similar neurodegenerative mechanisms seen in the secondary injury mechanisms of TBI suggesting a link worth researching [5]. Ultimately, as TBI continues to promote cell and tissue death and degenerate neuronal cells, it will also continue to pose as a high risk factor for several neurodegenerative diseases further highlighting the demand for increased research in the area of TBI.

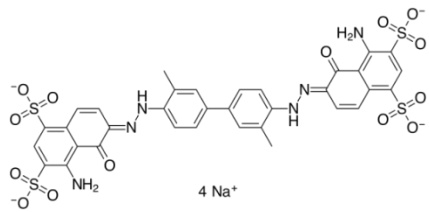
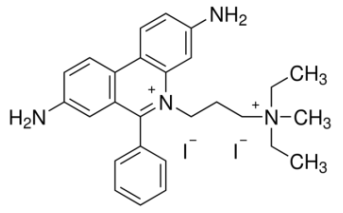
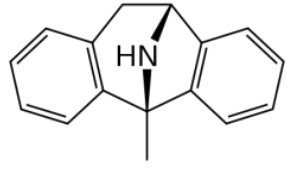
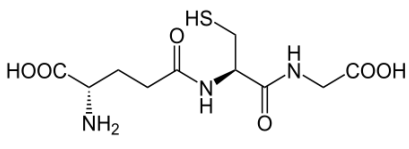
## **1.2 Specific Aims**

The first objective of this research project was to design a silk implant to locally deliver small molecule drugs to the brain over the course of 24 hours. The two drug delivery platforms tested were thin silk films and silk-HRP hydrogels. A small molecule dye, Evans Blue dye, was used to test the release kinetics of each design. Film parameters, such as silk concentration and water-annealing time, were tested in vivo in addition to different implantation techniques. Hydrogels of different heights were also tested in vitro and in vivo. A selection of these implants that displayed a minimal burst release and consistent transfer of dye into the cortex were used to release small molecule drugs.

The second objective was to load small molecule drugs into the silk implants, and determine their effects on decreasing cell death in brain tissue following a controlled cortical impact (CCI) model in mice. Only designs that showed success

in initial in vivo implantation were used. Small molecules loaded into implants included propidium iodide, dizocilpine, and glutathione (Table 1).

Table 1 Small molecule for delivery via silk implants

<i>Small molecule</i>	<i>Structure</i>	<i>Molecular weight</i>	<i>Function</i>
Evans Blue dye		960.81	Small molecule dye with red autofluorescence [8]
Propidium iodide (PI)		668.40	Red fluorescent cell death marker [9]
Dizocilpine (MK801)		221.30	Noncompetitive NMDA receptor antagonist [10]
Glutathione (GSH)		307.32	Antioxidant reducing agent [11]

## **2. Background**

### **2.1 Traumatic brain injury**

Traumatic brain injury (TBI) is a leading cause of death and disability worldwide accounting for approximately 2.2 million emergency department visits, 280,000 hospitalizations, and 50,000 deaths in one year in the United States alone, according to the Center for Disease Control and Prevention [1]. While the most effected populations include children, young adults, and the elderly, TBI remains highly heterogeneous in terms of etiology, severity, and outcome making it difficult to diagnose and treat [3]. The most common method for TBI classification immediately following injury is by the Glasgow coma scale (GSC) which ranges from 3-15 and consists of three components: eye, motor and verbal scales. Based on the score, injuries are classified as severe (GSC 3-8), moderate (9-13) or mild (14-15) [12]. Further assessment to determine structural damage via neuroimaging may be required depending on the initial score. Structural damage comes in various forms also known as primary injuries which are the result of the initial insult to the head [13]. A multitude of signaling cascades following primary injury and are known as secondary injuries which ultimately lead to cell and tissue death [14]. A variety of treatments exist, but most do not result in positive outcomes. Extensive research on neuropharmaceutical therapies is specifically being studied because of their ability to affect neurochemical signaling [15]. However, numerous challenges exist as pharmaceuticals make their way to clinical studies stressing a need to improve research methods at the preclinical level [16].

## **2.2 Primary injury**

Primary injury is the initial mechanical impact to the head and can result in the following immediate pathological features: concussion, skull fracture, contusion, contrecoup, diffuse axonal injury, hematomas, anoxia, hypoxia, and in infants, shaken baby syndrome [13]. Concussions are a brief interruption of neurological function following head trauma and may or may not include loss of consciousness. They are typically caused by acceleration and deceleration forces to the head [17]. Skull fractures can either be depressed where portions of the skull press against the tissue of the brain, or penetrating where pieces of the skull or another object breaks the tissue and enters the brain [13]. Contusions are caused by direct external contact forces or from the brain hitting the interior of the skull. They are often the result of more traumatic concussions [18]. Contrecoup injury is a type of contusion that is located diagonally opposite a skull fracture [19]. Diffuse axonal injury is produced by shear forces upon impact that generate nonuniform strains in the brain and subsequently stretches axons and small blood vessels. Hematomas are any bleeding around the brain and are classified as epidural, subdural, subarachnoid or intracerebral depending on the location of the bleed [18]. Anoxia is the complete lack of oxygen to brain tissue whereas hypoxia is the decrease of oxygen. Both occur despite adequate blood supply to the brain suggesting that mechanisms of oxygen absorption by the tissue are disrupted [13]. Lastly, shaken baby syndrome occurs when an infant has been violently shaken causing the brain to forcefully hit the inside of the skull. This severe injury leads to bruising, swelling, and bleeding of the brain [20].



## 2.3 Secondary injury

While primary injury occurs at the moment of impact of injury, secondary injury mechanisms may last hours to months to even years following initial insult. These mechanisms, or neurochemical signaling cascades, include the disruption of the blood-brain barrier (BBB), inflammation, oxidative stress, mitochondrial dysfunction, excitotoxicity, and finally neuronal apoptosis, or cell death [14]. Figure 1 provides an overview of the secondary injury signaling cascade following primary injury and Table 2 provides an overview of the most common primary injuries and their correlated secondary injuries, but most of these are simultaneously occurring to further exacerbate injury.

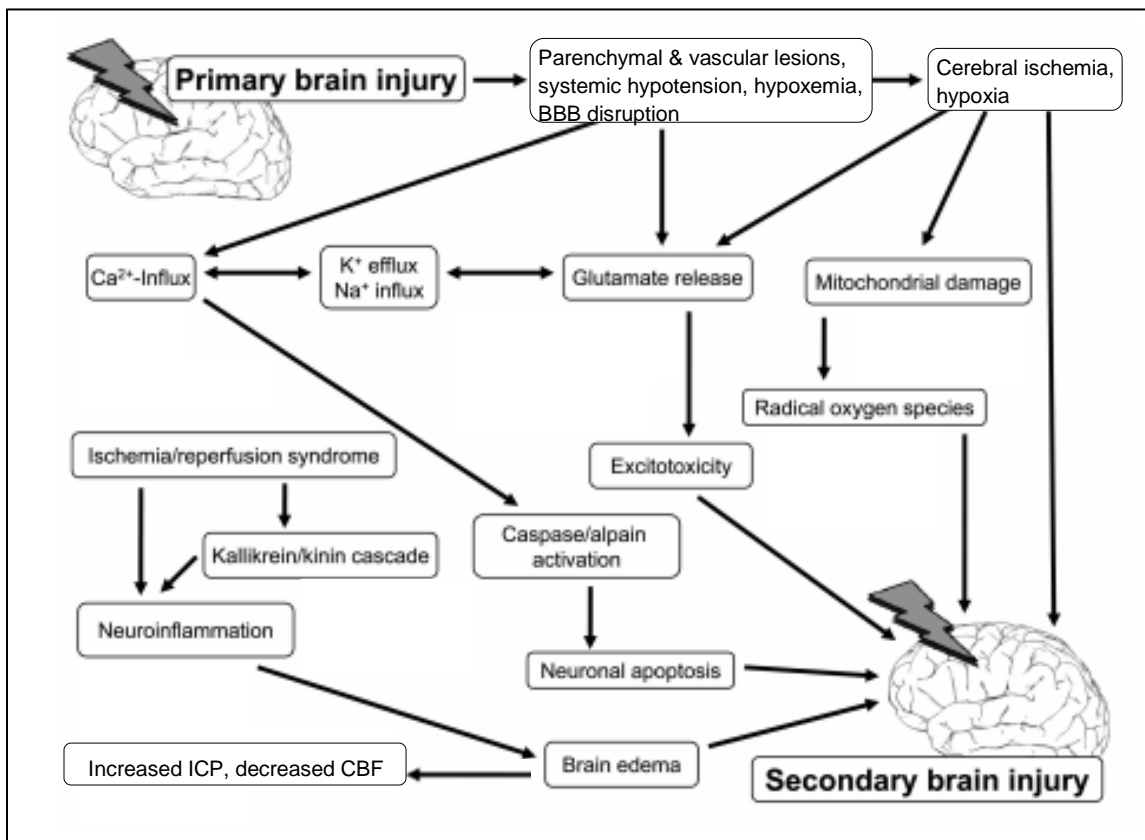


Figure 1 Secondary injury signaling cascade initiated by primary brain injury and leading to cell and tissue death [21]

Table 2 Major markers of TBI and their significance

<i><b>Physical markers of TBI (common 1<sup>st</sup> injuries)</b></i>	<i><b>Significance (common 2<sup>nd</sup> injuries)</b></i>
Skull fracture (penetrative damage)	BBB disruption
Edema (brain swelling)	Increased intracranial pressure (ICP), decreased cerebral blood flow (CBF), BBB disruption
Diffuse axonal injury (stretching of axons and blood vessels)	Oxidative stress, mitochondrial dysfunction, neuroinflammation
Hematoma (bleeding around the brain)	Neuroinflammation
Hypoxia (decreased oxygen supply)	Oxidative stress, mitochondrial dysfunction
Ischemia (decreased blood supply)	Mitochondrial dysfunction, neuroinflammation, decreased CBF

Furthermore, the duration of these effects offers a potential window for neuropharmaceutical therapy as opposed to other therapeutic options. At the onset of injury, the BBB is typically disrupted rapidly increasing its permeability. This induces cerebral edema due to the buildup of fluid as well as hypoxia and ischemia due to the inability of damaged blood vessels to supply blood and oxygen to brain tissues [21]. Additionally, because of the lack of nourishment, ATP production significantly decreases. This poor energy supply shuts down processes such as the sodium-potassium ATPase pump leading to a loss of membrane potential and homeostatic imbalance of ions [22]. There is an efflux of potassium ions and an influx of sodium and calcium ions [23]. In general, the movement of sodium and potassium initiates glutamate release and excitotoxic effects whereas calcium influx directly initiates oxidative stress and mitochondrial dysfunction, and cell death. Glutamate is an excitatory neurotransmitter, and one

of its primary receptors, the NMDA receptor, is a channel that allows both sodium and calcium ions to pass [24]. Calcium then activates a variety of cellular enzymes such as proteases, kinase phospholipases, calpains, and nitric oxide synthase all of which damage the integrity of cells [24]. Oxidative stress is brought on from nitric oxide synthase which promotes free radical formation. Highly reactive compounds, free radicals can further perpetuate cellular damage. Reactive oxygen species (ROS) levels in particular increase and cause oxidative damage. Mitochondria play a significant role in the energy deficit following injury, and with the increase of calcium and ROS, and calpain activation, the result is mitochondria dysfunction and the compromise of cellular function [22]. Additionally, when mitochondria undergo oxidative stress, they release apoptosis-inducing factor which as the name suggests induces apoptosis in neurons. Conversely, apoptosis can be induced with caspases (caspase-dependent apoptosis), with the aforementioned activation of calpains [25]. The last area for a potential therapeutic target is through the inflammatory response during cell death where leukocytes that have infiltrated the injured area release pro-inflammatory cytokines, oxidative metabolites and anti-inflammatory cytokines. The cytokines further induce apoptosis following TBI [26].

## **2.4 TBI management with neuroimaging and**

### **non-pharmaceutical therapies**

Neuroimaging plays a vital role in diagnosing TBI. Before selecting the best mode of treatment, the type and extent of injury must be determined. Ideally, computed tomography (CT) scans would be conducted on anyone sustaining minor head trauma, but in some cases it may not be necessary [17]. Some of these cases include when a patient is considered low risk meaning a GCS score of 15, no loss of consciousness, intact orientation and memory, and no other injuries among other factors [17]. The need for neuroimaging increases with medium and high risk patients. Behavioral and cognitive examinations alone fail to provide information on physiological damage within the brain that may result in delayed effects. Skull radiographs may also be conducted in the absence of a CT or before making further decisions to continue advanced neurotrauma management. Skull radiographs are capable of revealing fractures, fluid in the sinuses, and possible penetrating objects [17]. However, CTs can reveal more detailed information on contusions, hematomas, diffuse axonal injury, intracranial hemorrhages and other types of injury. Because of this, CTs are the preferred method of assessment, but also because of their accessibility and speed [27]. MRIs also provide valuable information, but require a much longer period of time. They are more valuable to determine prognosis once initial treatment is established from CT results [28]. Technologies in nuclear medicine particularly with SPECT and PET are also emerging in the process of developing treatment plans for TBI patients. Single positron emission computed tomography (SPECT) requires relatively little time

and can also generate 3D data. They can be used to assess brain blood flow and regional brain metabolism using a radioactive tracer material. Positron emission tomography (PET) imaging can also assess regional brain metabolism as well as local brain damages [27]. Although all modes of imaging are vital and extremely valuable, they do not treat the negative effects of TBI. However, the added information nuclear medicine provides to traditional imaging techniques allows for emergency physicians to determine the best option for treatment and prevent further damage.

Before neuropharmaceuticals became a heavily researched therapy for TBI, and while translational challenges are currently being addressed, nonpharmacological therapies exist to relieve the negative effects of TBI. Following the assessment of CT or MRI scans, physicians may choose one or more treatments including a decompressive craniectomy, hypothermia, or hyperosmotic therapy among others [3]. The primary reason to begin management immediately following injury is to prevent hypoxia and hypotension which lead to secondary brain damage [29]. Prior to being admitted to a hospital, decreased oxygen and hypotension can be treated via endotracheal intubation and IV fluid (saline) respectively [12]. High ICP can also be minimized shortly following injury by inducing hyperventilation. This is accomplished by inducing cerebral vasoconstriction and the reduction of cerebral blood flow [12]. Once at the hospital, more invasive therapies become available. ICP monitoring by means of a catheter, placed within the ventricles of the brain, connected to an external pressure transducer is not only a very accurate

way of measuring ICP, but it also provides a route to drain cerebral spinal fluid (CSF) which subsequently decreases ICP [12]. Intravenous delivery of intermittent doses of mannitol is also an effective agent in reducing ICP as a form of osmotherapy. It creates an osmolar gradient which generates the movement of water across the BBB and improves focal CBF [29]. Other means of reducing ICP are with a decompressive craniectomy or hypothermia. Decompressive craniectomies are commonly performed to treat brain swelling. This procedure consists of the removal of a section of the skull which allows the brain to expand and the ICP to decrease. Although this method is thought to bring about overall positive outcomes, there have been contradicting results making it a last resort means of therapy when other treatments to reduce ICP have failed. Researchers claim there is a lack of therapeutic effect because neither the timing of this surgery nor its role in secondary brain injury has been studied extensively [29]. Hypothermia is used in few cases as more animal studies are being conducted to determine the overall benefits of its therapy [3]. It has shown to reduce brain metabolic rate, affect CBF, reduce critical threshold for the delivery of oxygen, block excitotoxic mechanisms, block calcium activity, decrease edema formation, and modulate apoptosis. Because of its multi-faceted effects, hypothermic therapy may open more avenues for pharmacological treatment. Currently research is also being focused on localized cooling treatments such as surface cooling, intranasal selective hypothermia, extraluminal vascular cooling and epidural cerebral cooling [30].

## **2.5 Neuropharmaceutical therapy**

Unfortunately, despite great advancements in the pharmaceutical industry, drugs intended for the CNS have one major obstacle that medications to other sites of the body do not encounter – the blood brain barrier (BBB) [31]. This barrier consists of capillary endothelial cells that protect the brain from toxic substances, but efficiently allow the passing of oxygen, glucose, and other nutrients [32]. Attempts to delivery drugs to the brain can be categorized into three main routes: intravascular, intracerebral, and intraventricular [33]. Studies have shown that, of the drugs administered intravascularly, or systemically, 98% of small molecules (those with a molecular weight greater than 500 Daltons) do not pass the barrier and nearly all large molecules ( $MW > 1$  kilodaltons) fail to reach their destination [34]. Strategies to pass the BBB systemically include generating an osmotic imbalance and manipulating endogenous transport systems. The use of hyperosmolar substances shrinks endothelial cells and open tight junctions allowing for lipophilic molecules to enter, but this technique has mostly been used to treat brain tumors. Transport systems for glucose, neutral amino acids, and some peptides can be utilized to generate carrier-mediated uptake systems where desired drugs can enter the brain with assistance from one of these endogenous pathways (Figure 2) [33].

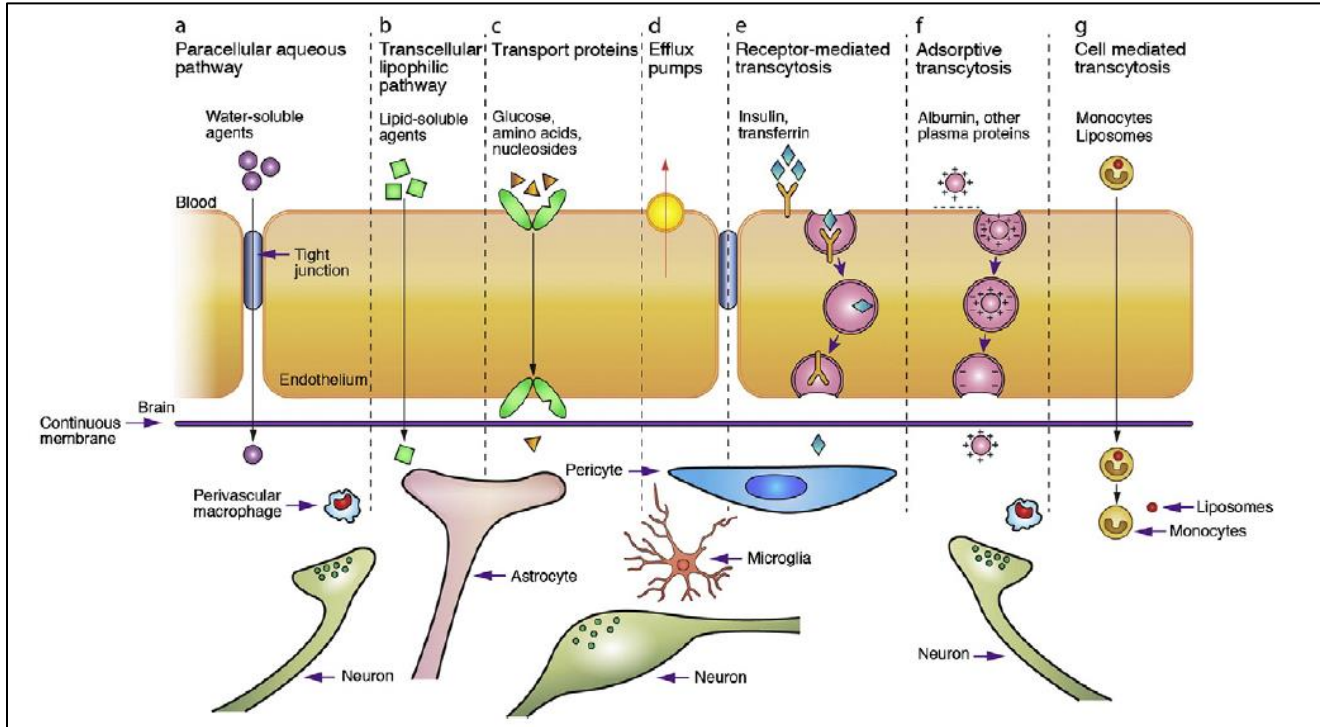


*Figure 2* Overview of transport routes through the blood brain barrier via endogenous pathways. a) paracellular aqueous pathway; b) transcellular lipophilic pathway; c) transport proteins; d) efflux pumps; e) receptor-mediated transcytosis; f) adsorptive transcytosis; g) monocytes and liposomes [35]

During intracerebral delivery, molecules can directly enter the brain parenchyma via intrathecal catheters or controlled release matrices among a few other routes. The fundamental problem with this strategy is the diffusion coefficient of each molecule attempting to enter the brain. Because of the complexity of the parenchyma and its gray and white matter, molecules have minimal movement from the location they are initially released, and consequently their diffusion coefficients are on the order of  $10^{-6}$  cm/s [33]. This mode of delivery is difficult to pursue for TBI patients because of the narrow therapeutic window following injury. Lastly, during intraventricular delivery, there is potential for cerebral spinal fluid (CSF), which freely moves into the parenchyma, to carry drugs. From



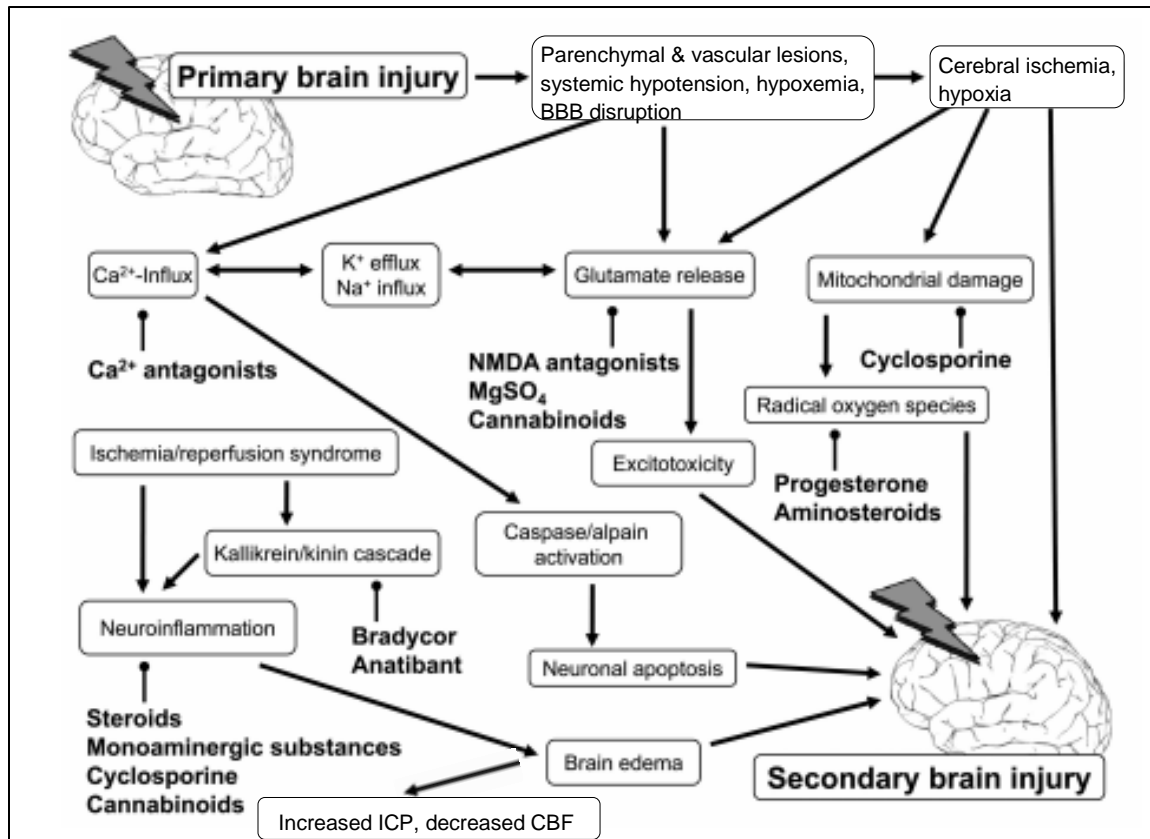
this point, these small molecules would be able to diffuse into the brain. Again, as previously mentioned, the diffusion rates of drugs are extremely slow, and the much faster clearance rate of CSF works against successful delivery [35]. Increased diffusion rates to that comparable to CSF clearance rates could potentially make intraventricular delivery an option for drug delivery capable of creating a therapeutic effect. The challenges addressed here are for an intact brain and the scenario becomes vastly more complicated in injured brains.

In the case of TBI, the BBB is disrupted and it is expected for small molecules to successfully enter the brain parenchyma with this barrier appearing to no longer be an issue. Unfortunately, disruption of the BBB is more complex, as described earlier with respect to secondary injury, and makes drug delivery to the brain more challenging. Following injury, the breakdown of the BBB is biphasic meaning that is open for a period of time before closing, and this time period is dependent on the severity and duration of the insult [33]. If a drug is to be administered, it would not only have to be delivered within this window, but also diffuse into the brain parenchyma, and as mentioned before the majority of tested molecules have extremely slow diffusion rates. Thus, the likelihood of successful delivery before the BBB closes is quite low. Moreover, TBI is often multi-focal, and as a result, areas deeper in the brain that are subject to secondary injury may still have an intact BBB. Therefore, drugs entering the brain at the site of primary injury may still come into contact with an intact BBB in other regions [33]. Also following injury, CBF decreases. This makes intravascular delivery ineffective

because a minimal amount of blood would be available to carry drugs to the brain. Intraventricular delivery also becomes ineffective as ICP increases during edema and creates an obstacle for successful drug diffusion. Research on drugs to stabilize the BBB and to circumvent decreased CBF and increased ICP is ongoing with slow progress [36].

## **2.6 Sites for therapeutic intervention**

Each secondary injury pathway has several neuroprotective and neurorestorative therapeutics that have been used in an attempt to prevent cell and tissue death and/or promote restoration of cells and tissues following injury. Common neuroprotective strategies include calcium-channel blockers, corticosteroids, excitatory amino acid inhibitors, NMDA receptor antagonists, free radical scavengers, magnesium sulfate, growth factors, and inflammatory modulators among numerous others (Figure 3) [15]. Table 3 lists several other common neurotherapeutics and potential sites for therapeutic intervention or mechanism of action. The majority of compounds listed here primarily target the signaling cascade initiated by the influx of calcium, NMDA receptors to prevent the binding of glutamate, free radicals to minimize their effects, or cell death via the inflammatory response.



Neurorestorative measures are also becoming increasingly prevalent in treating traumatic brain injury because recent preclinical studies have indicated that within a period of time, TBI induces neurogenesis, angiogenesis, axonal sprouting, and synaptogenesis [30]. As neuroprotective therapeutics prevent further cell and tissue death, neurorestorative therapeutics should be seen as equally important in order to promote cell and tissue growth and healing during this window after injury. Common therapeutics for this purpose includes erythropoietin, statins, bone marrow stromal cells, and nitric oxide [30]. Unfortunately, despite the extensive amount of research conducted on drug discovery for the treatment of

TBI, over 30 phase III clinical trials that have showed some promise have failed. Many of these have used a single-target approach focusing on one aspect of the secondary injury signaling cascade [37]. The combination of neuroprotective and neurorestorative strategies may serve to better therapeutic outcomes.

*Table 3* Current neuropharmaceuticals and sites for therapeutic intervention

<b><i>Neuropharmaceutical</i></b>	<b><i>Expected mechanism of action following TBI</i></b>
Antioxidants and free-radical scavengers	Replenishes endogenous antioxidants reduced following trauma [38]
Barbiturates	Reduces ICP [30]
Calcium channel antagonists	Reduces regional cerebral edema [15]
Cannabinoids	Inhibits release of glutamate and inflammatory cytokines [23]
Cell cycle inhibitors	Inhibits cell cycle activation, neurodegeneration and chronic neuroinflammation; activates microglia and astrocytes [16]
Cyclosporin A	Preserves mitochondrial function; inhibits lipid peroxidation and oxidative stress [16]
Diketopiperazines	Reduces calpain [16]
Erythropoietin	Limits excitotoxic, pro-oxidant and inflammatory effects [16]
Gangliosides	Promotes neurite sprouting and growth; reduces NMDA receptor-mediated release of excitatory amino acids [38]
Glutamate (NMDA) receptor antagonists	Improves neurological function; recovers magnesium ion homeostasis [38]

*Table 3 Current neuropharmaceuticals and sites for therapeutic intervention (continued)*

<b><i>Neuropharmaceutical</i></b>	<b><i>Expected mechanism of action following TBI</i></b>
Magnesium ion ( $Mg^{2+}$ )	Improves cerebral metabolism and neurobehavioral outcomes [15]
Metabotropic glutamate receptor-5 agonists	Reduces expression of inducible NO synthase, production of NO and intracellular generation of ROS; limits caspase [16]
Minocycline	Inhibits glutamate receptors, neurotoxicity, pro-inflammatory cytokines; promotes microglial activity [26]
Modulators of arachidonic acid metabolism	Improves cerebral metabolism, blood flow and neurological function; Reduces BBB permeability and cerebral edema [15]
Opioid receptor antagonists	Improves CBF; reduces ischemia; limits changes in calcium ions [38]
Platelet activating factor antagonists	Improves neurological score and mitochondrial respiration rate; inhibits regional edema [15]
PPAR agonists	Inhibits pro-inflammatory cytokines, oxidative metabolites and edema; promotes anti-inflammatory cytokines [26]
Progesterone	Reduces glutamate excitotoxicity, membrane lipid peroxidation, apoptotic and inflammatory pathways, and diffuse axonal injury [16]
Recombinant factor VIIa	Limits intracerebral hemorrhage [30]
Statins	Reduces glial cell activation and cerebral edema; restores BBB integrity [16]
Steroids and inhibitors of lipid peroxidation	Inhibits lipid peroxidation; limits edema [38]
Substance P antagonists	Reduces inflammation; maintains BBB integrity [16]
SUR1-regulated $NC_{Ca-ATP}$ channel inhibitors	Reduces edema, secondary hemorrhage, inflammation, apoptosis and lesion size [16]
Thyrotropin-releasing hormone	Increases CBF and metabolism; decreases platelet-activating factor, endogenous opioids and glutamate [16]

## **2.7 Challenges from translating between preclinical and clinical studies**

The primary reason neuropharmaceutical research for TBI has seen little success is because of the challenges in translating from preclinical to clinical studies. Preclinical studies have largely focused on the types of molecules that affect the various secondary injury mechanisms. While this aspect is absolutely necessary in the path to drug discovery, data from several other preclinical components are essential before seeing positive therapeutic effects in clinical trials. These additional results include determining the optimal route of administration, the pharmacokinetics and pharmacodynamics of each molecule, the proper therapeutic window to deliver the drug, whether a single or multiple dosage is required and whether a bolus or continuous dose should be administered [14]. However, before even these results can be collected, designing animal models that more closely mimic injury has become a top priority. Animal models, with both small and large animals, already are inherently difficult to utilize to study brain injury in humans because the biomechanics of injury such as in rotational loading is difficult to scale between animals and humans [39]. Even when a close correlation is determined, there are very few ways to properly evaluate cognitive and psychiatric impairments. Furthermore, as previously mentioned, TBI is extremely heterogeneous and current animal models do not encompass their complexity because they are designed to be highly controlled to maintain consistency [40]. Continued research using animal models must be modified to capture the multi-faceted nature of brain injury. A large modification includes

using a multiple-injury model in addition to observing the results from a variety of single-injury models which has been the current approach. Although much effort would be required to control these experiments, multiple-injury models would mimic human brain damage to a greater extent [41]. Additionally, these models should address the various demographics of the population of TBI patients particularly age and sex. The consequences of injury vary depending on if a patient is adolescent or elderly and also if the patient is female or male according to some previous studies [41]. Updated animal models should include these factors when improving injury models to obtain more extensive results. Once improved models are established, there is also a need for long-term studies. Whereas short-term studies are beneficial for understanding the acute stages of injury, long-term studies would allow a deeper look into the delayed secondary injury mechanisms. More importantly, these studies could verify if changes in the acute stages could predict outcomes in later stages which would markedly assist clinicians in determining treatment [14]. Long-term studies would also help define much needed biomarkers to measure functional outcomes. The heavy research being conducted on discovering neuropharmaceuticals for the treatment of TBI is likely failing because minimal data are being collected from inadequate animal models for only short periods of time and not only because the specific molecules being tested do not have a therapeutic effect. Thus modifying the overall design of TBI research is crucial to address the translational challenges between preclinical and clinical studies.

### **2.7.1 Common animal models for TBI**

#### *2.7.1.1 Control cortical impact (CCI)*

CCI injuries are used to study focal injuries. As an open head injury model, CCI is induced using an impact device driven by high pressure or electromagnetism to force a rigid impactor onto an intact dura exposed by a craniotomy [40]. This injury mimics cortical tissue loss, acute subdural hematoma, axonal injury, concussion, and BBB disruption. CCI is very common because of its control over time, velocity and depth of impact [41]. However, this model also comes with several disadvantages. Along with inducing a contusion, there is also extensive damage to the ipsilateral cortex which is not comparable to human injuries. Secondly, the bone flap must be replaced following the craniotomy. Otherwise brain swelling may actually be alleviated as seen in decompressive craniectomies which is not preferred when using an injury model. Lastly, CCI does not damage the brain stem and produce unconsciousness which again does not mimic human brain injury [40].

#### *2.7.1.2 Weight-drop injury (WDI)*

Weight drop induced injuries are also used to study focal injuries. In this closed-head injury model, a free-falling weight is dropped onto the exposed skull [40]. The severity of the injury is adjusted by altering the height from which the weight falls and the mass of the weight. The model is particularly useful for producing diffuse axonal injury (DAI). Although injury severity is rather difficult to maintain constant, the DAI produced closely mimics the injury seen in humans



[41]. A prominent limitation to WDI is that it also delivers a second impact from a rebound hit [40].

#### *2.7.1.3 Fluid-percussion injury (FPI)*

FPI models are used to study diffuse injuries [40]. In this open head injury model, a pendulum strikes the piston of a reservoir of fluid to produce a fluid pressure pulse that impacts the dura exposed by a craniotomy. The fluid percussion pulses deform and displace the brain tissue [41]. Injury severity is controlled by altering the strength of the pulse. FPI is successful in mimicking TBI without skull fracture along with intracranial hemorrhage and brain swelling. The limitation of FPI is variability – the placement of the craniotomy is crucial to maintaining control of the model in order to minimize differences in pathological and behavioral outcomes [40].

## **2.8 Silk implants for localized drug delivery**

Despite improvements in drug-eluting implants and injections, local delivery of drugs following a variety of surgeries still remains the topic of drug delivery research. Delivery to the brain, particularly through intravascular, or systemic delivery, requires repetitive dosing at high concentrations resulting in negative side effects such as renal and liver failure [42]. Such complications further worsen a patient's condition impeding convenience and escalating cost of care [43]. Additionally, tissue damage following surgery gives rise to insufficient CBF at the site decreasing the effectiveness of systemic delivery [44]. Highly

prevalent, these risky drawbacks necessitate the demand for improved localized delivery via either the intraventricular or intracerebral routes through which neuropharmaceuticals can provide optimal therapeutic effects.

Among the most successful natural polymers is silk fibroin, specifically from the *Bombyx mori* silkworm cocoon. The protein boasts several qualities making it a very useful material for in vivo and in vitro studies of both bulk and sustained release of drugs. These include biocompatibility, biodegradability, and extraordinary tunability of its chemical and mechanical properties [45]. Furthermore, silk fibroin can be processed in aqueous systems under mild temperatures and pressures creating a viable environment for a plethora of compounds and proteins while maintaining their bioactivity [46]. This protein has shown to be non-toxic and non-immunogenic while currently being applied to wound-healing, surgical sutures, and blood-vessel regeneration [47]. The incorporation of drug delivery following surgery into these silk-based applications is a growing area of research, but has yet to be used to treat the secondary injuries following TBI.

As a host for drugs, silk fibroin inherently possesses numerous advantages over its competing polymer drug reservoirs. While these polymer reservoirs require processing environments detrimental to bioactive molecules (i.e. heat, extreme pH, shear stress), silk protein operates in more ambient conditions withstanding a range of temperatures and allowing ease of transfer between room and body

temperatures [48]. Moreover, whether through implants or injections, silk platforms offer flexible pharmacokinetics for localized delivery through control of its physical and chemical properties. Existing polymers lack such flexibility thereby eliciting the need to increase drug dosages [43]. However, as stated previously with systemic modes of delivery, high dosages pose adverse effects. Silk's ability to deliver drugs in healthy dosages directly to the surgical site minimizes this risk while maximizing efficacy. Research has also shown that silk enhances the bioactivity of the drugs it encapsulates through thermal and storage stability [47].

Dosage requirements are determined by studying drug pharmacokinetics which are directly correlated to the interaction of the physiochemical properties of silk fibroin and the drug of choice. Two specific control points are the molecular weight of the drug and the crystallinity of the silk polymer. Both affect the primary variable of kinetics, the diffusion coefficient [49]. Molecular weight can be controlled by means of altering the drug's morphology such as its geometry, thickness of coatings if any exist, and porosity. Compounds with lower molecular weights are expected to diffuse easier through the matrix and have higher diffusion coefficients. Crystallinity of the silk matrix is controlled through beta-sheet content of the silk fibroin protein therein affecting the permeability of biomolecules and the rate of diffusion [48]. Lower crystalline structures allow molecules to permeate the matrix easier, again with a higher diffusion coefficient [49]. Thus by adjusting the molecular weight of the drug and the crystallinity of

the silk platform, the rate of diffusion can be controlled to achieve desired release patterns. In addition to rate of diffusion, rate of degradation of the silk polymer is an alternative to regulating release [48]. This option arises during instances when the structure of the drug does not allow the drug itself to diffuse easily despite decreased silk crystallinity (i.e. when the altering of the drug's structure hinders the drug's effect). Higher molecular weight structures lack the tendency to diffuse unlike their lower molecular weight counterparts, and therefore more heavily rely on degradation of the silk carrier to liberate the drug. Again, along with silk concentration and porosity, degradation time is regulated via beta sheet content which can be manipulated via methanol treatment or water-annealing processes to control the degradation of silk within a span from weeks to years [43]. For better local delivery, both the diffusion and degradation of drug and silk platform, respectively, may be regulated to ensure that proper dosages permeate the matrix while extending the duration of therapeutic effect.

Before pharmacokinetics can be measured, drugs must be loaded into one of the many silk formats. Typically, loading a drug into a polymer is accomplished by one of three ways: (1) 'bulk loading' of the drug by mixing the drug into the silk solution before processing; (2) surface decorating of the platform through chemical coupling or adsorption; or (3) use of composite systems such as a combination of different silk platforms or a combination of silk with another natural or synthetic polymer [48]. Each of these methods is theoretically suitable for each of the multitude of silk delivery platforms – microspheres, sponges,

hydrogels, or films – though more research is required to better understand release rates once drugs are loaded.

### **2.8.1 Thin silk films**

Silk films as a platform for the delivery of bioactive molecules have shown great potential because of the film's ability to stabilize and enhance the compounds it encapsulates [46]. Some processing options include slow drying, water annealing, stretching, compressing, and solvent immersion all of which control the mechanical properties of the film [48]. In the context of neurological applications, thin silk films have been utilized to support neuron-electrode interfaces where electrodes are embedded within film implants. These thin silk films implanted in mice are able to conform to the brain's curved surface with minimal inflammatory response [50]. A similar design was selected for this project with the expectation that the film's contact with the surface of the brain would allow maximum delivery of small molecules. Specifically in this research, the release of bulk-loaded small molecules is controlled by varying silk concentration and water-annealing time. Where silk concentration affects final film height, water-annealing induces the beta sheet formation in silk fibroin. As previously described, these parameters contribute to the crystallinity of the silk matrix and the rate silk films dissolve to consequently release small molecules.

### **2.8.2 Silk-HRP hydrogels**

Hydrogels prepared with silk fibroin exhibit great physical properties which is beneficial for implantation into a range of surgical sites. Their formation can be induced by several methods such as through manipulating pH, temperature, and shear forces, or through vortexing, electricity, and sonication [51]. Hydrogels also possess a unique quality in that gelation can be controlled to prolong the liquid state of the silk solution and the release of drugs [48]. Drug release from silk hydrogels is characterized by a rate-limiting step which can either be diffusion-based or swelling-based [51]. In the context of the physiological conditions of the brain, release from silk-HRP hydrogels is expected to be diffusion-based. Due to the high salt concentration of CSF, hydrogels are not expected to swell, but rather release small molecules along with the outward flow of water from the hydrogels [52]. In this project, hydrogels are prepared by enzymatically crosslinking silk fibroin catalyzed by horse-radish peroxidase (HRP) and hydrogen peroxide ( $H_2O_2$ ). Where beta-sheet content controls the release rate from films, beta-sheets make silk hydrogels brittle hindering proper gelation. Enzyme-catalyzed crosslinking for the formation of silk hydrogels requires phenolic groups which are found on the tyrosine side chains in silk fibroin. The addition of HRP and  $H_2O_2$  generates tyrosine radicals which then react to form dityrosine bonds, or crosslinks [52]. Thus, in addition to silk concentration and silk boiling time, gelation is also controlled by the concentrations of HRP and  $H_2O_2$ . These parameters inherently alter gel thickness, but the volume of solution was also used for further control of release.

### **3. Materials and Methods**

#### **3.1 Silk fibroin extraction**

Silk fibroin was harvested from *Bombyx mori* silkworm cocoons (Tajima Shoji Co. LTD, Sumiyoshicho, Naka-Ku, Yokohama, Japan). After cocoons were cut, they were boiled (45 minutes for films and 30 minutes for hydrogels) in 0.02M Na<sub>2</sub>CO<sub>3</sub> (Sigma Aldrich, St. Louis, MO, USA), and then rinsed three times in 20 minute cycles to ensure the removal of sericin proteins. The remaining silk fibers were left to dry overnight. The dried silk was dissolved in a 9.3M solution of LiBr (Sigma Aldrich, St. Louis, MO, USA) for 4 hours at 60°C. The solution was injected into 12-30mL Slida-A-Lyzer dialysis cassettes (Pierce, Woburn, MA, USA) and then suspended in water. The water was changed six times over the course of 48 hours. After this period, the resulting silk solution was removed from the cassettes and centrifuged at 10,000 rpm and 4°C for two 20 minute cycles or until impurities were removed. The final concentration by weight/volume (w/v) was calculated by dividing the weight of a sample of dried silk solution by the initial volume of the sampled solution.

#### **3.2 Polydimethylsiloxane (PDMS) molds**

A Sylgard 182 Silicon Elastomer Kit was purchased from Dow Corning (Midland, MI, USA). Base and curing agent were mixed well in a 10:1 ratio respectively. Solution was then poured into plastic petri dishes just enough to cover the bottom surface. Dishes were lightly covered in foil and placed on a flat surface in a 60°C oven for approximately 1 hour. Dried PDMS molds were removed from the oven,

wrapped in foil and stored at room temperature until needed. Biopsy punches (Integra Miltex Standard Biopsy Punch, Plainsboro, NJ, USA) of 4mm in diameter were used to cut out 4mm posts from the larger PDMS mold. The posts were placed in another dish under a cell culture hood to maintain a sterile environment.

### **3.3 Casting films**

Silk films were prepared by adding a total volume of 13 $\mu$ L of silk with concentrations of 2% and 5% w/v to the PDMS posts to produce films approximately 50 $\mu$ m and 80 $\mu$ m in height, respectively. Silk was first filtered to remove minor impurities and enhance sterility using a Whatman PES sterile filter (GE Healthcare UK Limited, Amersham Place, Little Chalfont, Buckinghamshire, UK). Small molecules loaded into films were mixed into the filtered silk solution to maintain the desired silk concentration and total film volume. Once solution was casted onto PDMS posts, they were left to dry overnight before water-annealing. Films were water-annealed via a desiccator which was set up with sterile water under the cell culture hood and attached to the house vacuum (20-25mmHg) to induce beta sheet formation in the silk.



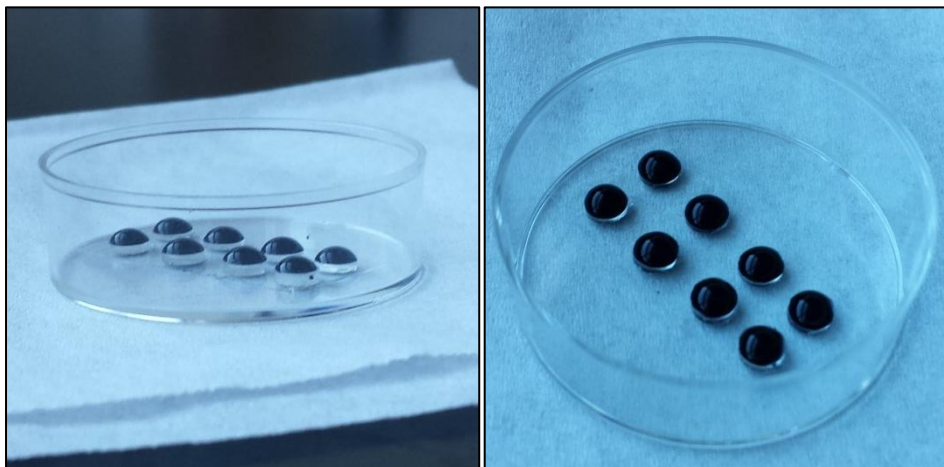


*Figure 4* Silk films (4mm in diameter) loaded with Evans Blue dye drying on PDMS molds.



*Figure 5* Desiccator arranged to water-anneal silk films with a vacuum pressure of 20mmHg.

### **3.4 Enzymatically cross-linked hydrogels**

Hydrogels were prepared by crosslinking horse-radish peroxidase (HRP) and hydrogen peroxide ( $\text{H}_2\text{O}_2$ ) with 5% w/v silk fibroin solution. A 1000 unit/mL HRP solution was produced by adding distilled water to the solid powder initially provided with a concentration of 200-300 units/mg (Sigma Aldrich, St. Louis, MO, USA). Water and powder was gently mixed to form a proper solution and stored at 4°C when not in use. A 1% w/w  $\text{H}_2\text{O}_2$  solution was prepared from a 30% w/w stock solution by making a 1:30 dilution in distilled water (Sigma Aldrich, St. Louis, MO, USA). The diluted solution was prepared fresh before each use during hydrogel production. A silk-HRP hydrogel solution was finally prepared by first mixing 1mL of filtered silk solution with 10 $\mu\text{L}$  of HRP solution followed by 10 $\mu\text{L}$  of hydrogen peroxide solution (a 100:1:1 ratio). Small molecules were added to maintain a 5% w/v silk concentration just before the addition of  $\text{H}_2\text{O}_2$  which initiated gelation. The final solution was briefly vortexed to ensure a homogenous suspension of drug. A range of volumes of solution was cast onto PDMS posts to create hydrogels of different heights. Once casted, the solution was left to gel and dry overnight.

#### **3.4.1 In vitro release**

The release of 100 $\mu\text{g}$  of Evans Blue dye from silk-HRP hydrogels of different heights (80 $\mu\text{m}$ , 120 $\mu\text{m}$ , 180 $\mu\text{m}$ , 200 $\mu\text{m}$ ) was tested in a 48-well plate. Each well was filled with 1mL of 1x phosphate buffer solution (PBS) and 3 100 $\mu\text{L}$  samples were collected from each well for each time point into a 96-well plate. Using a

UV-vis spectrophotometer (SpectraMax M2, SunnyVale, CA, USA), the absorbance of dye was measured for each time point (Excitation/emission = 540/640nm). Measured absorbance values were compared against a standard release curve of dye to determine the dose of dye released at each time point.

### **3.5 In vivo subjects**

All procedures were approved by the Institutional Animal Care and Use Committee of the Massachusetts General Hospital and were in compliance with the National Institutes of Health guidelines for the care and use of laboratory animals. Adult C57 black 6 mice (Jackson laboratories, Bar Harbor, ME) were given access to food and water and housed in a temperature-controlled room with a 12-hour light/dark cycle.

### **3.6 Surgical implantation**

An in-depth description of the craniotomy can be found in previously published work [53]. Briefly, mice were anesthetized with 4.5% isoflurane (Anaquest, Memphis, TN) in 70% N<sub>2</sub>O and 30% O<sub>2</sub> using a Fluotec 3 vaporizer (Colonial Medical, Amherst, NH). Blow-by anesthesia was maintained with 4.5% isoflurane for the duration of the surgery. This procedure and rationale for anesthesia produces unresponsiveness to tail and toe pinch and to surgical procedures, but maintains blood pressure and blood gases within normal limits. After being initially anesthetized, mice were positioned in a stereotaxic apparatus to stabilize their heads. The skull was exposed with a midline scalp incision. PBS

was used to moisten the surgical area before using a hand drill and trephine to perform a 5mm craniotomy of the parietal bone. A Q-tip was used to dry the exposed area from CSF and any blood. Silk implants were then locally placed on the dura above the parietotemporal cortex. The removed section of bone was also dried and returned to the skull. At this point, the head was either both closed and sutured, or the bone flap was sealed with an adhesive, cyanoacrylate (surgical bone glue), before closing (Vetbond, 3M, St. Paul, MN, USA). Figures 6 and 7 display two methods for applying an adhesive. The temporary method in Figure 6 applied cyanoacrylate to the bone flap to provide a slight amount of pressure. The final method for implantation is depicted in Figure 7 where a 4mm by 4mm steri-strip (3M, St. Paul, MN, USA) was cut and applied to the bone flap followed by the placement of a small piece of cotton to ensure transfer of drug to the brain. After suturing the incision, mice were then removed from under anesthesia and returned to their cages for 24 hours.

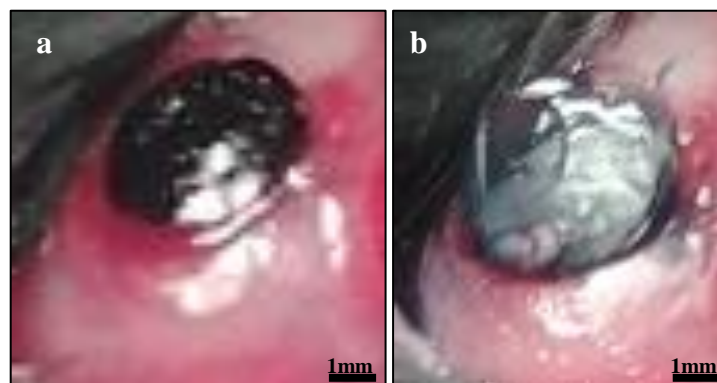


*Figure 6* a) Thin silk film implantation b) Replacement of bone flap sealed with cyanoacrylate

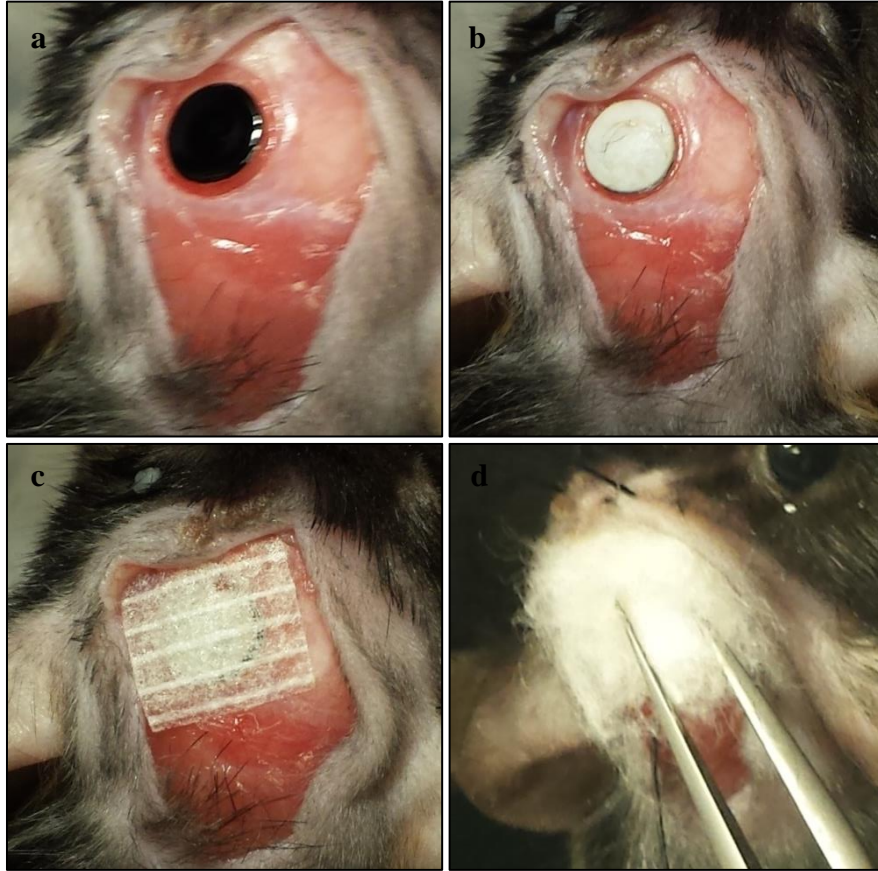


*Figure 7* a) Silk-HRP hydrogel implantation b) Replacement of bone flap  
c) Application of steri-strip d) Placement of cotton

### **3.7 Controlled cortical impact (CCI)**

A description of performing CCI can be found in previously published work [53]. Briefly, CCI was used to induce a cerebral contusion following implantation of the silk drug delivery vehicle and transfer of the drug to the brain. Mice were again anesthetized with 4.5% isofluorane in 70% N<sub>2</sub>O and 30% O<sub>2</sub> using a Fluotec 3 vaporizer. Blow-by anesthesia was maintained with 4.5% isofluorane for the duration of the surgery. After being initially anesthetized, mice were situated in the CCI apparatus with their heads again stabilized. The applied pressure from the cotton was removed along with the steri-strip. Impact was delivered using a 3mm

flat tip pneumatic piston at a velocity of 6m/s, duration of 100ms, and depth of 0.6mm. The piston was centered on the dura and the brain compressed until the impactor was flat on the brain surface. Mice were sutured and returned to their cages to recover from anesthesia.

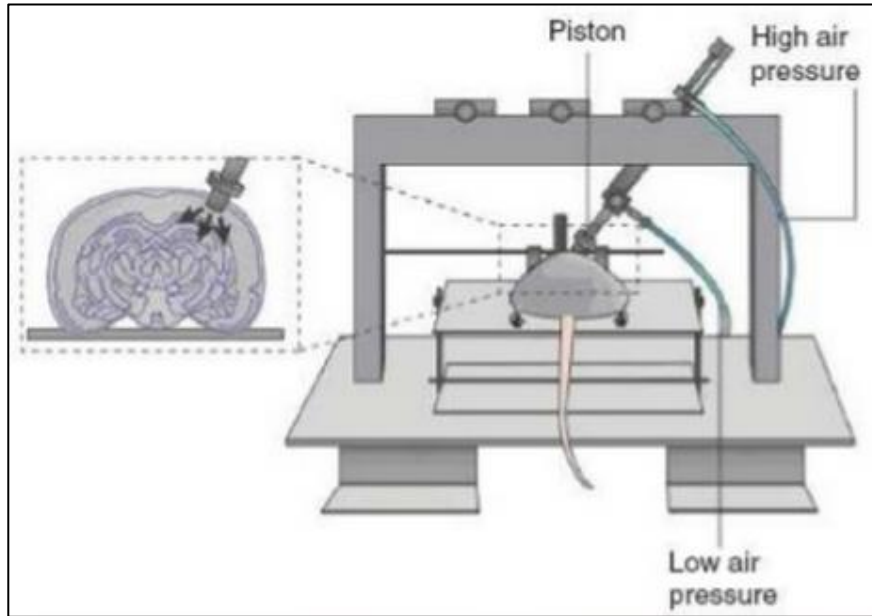


*Figure 8* Apparatus for controlled cortical impact. High air pressure is applied to a piston initiating impact direction onto the dura [42]

### **3.8 Sample preparation**

One hour following CCI, mice were again deeply anesthetized and decapitated. Brains were removed and stored at  $-80^{\circ}\text{C}$ . Brain sections on glass microscope slides were prepared on a cryostat with  $12\mu\text{L}$  slices made every 1mm. Slides were immersed in absolute ethanol for 5 minutes before they were coverslipped. The sections were imaged under a fluorescent microscope (Nikon Eclipse Ti, Avon, MA).

## **4. Thin Silk Films**

### **4.1 In vivo results**

#### **4.1.1 Single film implants**

Thin silk films loaded with 100 $\mu$ g of Evan Blue dye were initially brought to a final concentration of 2% w/v. A total volume of 13 $\mu$ L was used to bring films to an average height of 50 $\mu$ m. The goal was to determine the effect of water-annealing time in vivo by observing the transfer of dye onto the dura of mouse brains. Implanted films were water-annealed for 1, 3, 4 and 5 hours (Figure 9). In addition to inconsistent dye transfer from mouse to mouse, films that displayed minimal transfer onto the dura failed to penetrate the cortex as seen in the fluorescence microcopy images. Slightly thicker films loaded with the same concentration of dye were brought to a final concentration of 5% w/v. The average height of these films was 80 $\mu$ m. Implanted films were annealed for 5 hours (Figure 10). Again, little to no transfer was observed for all implantations.



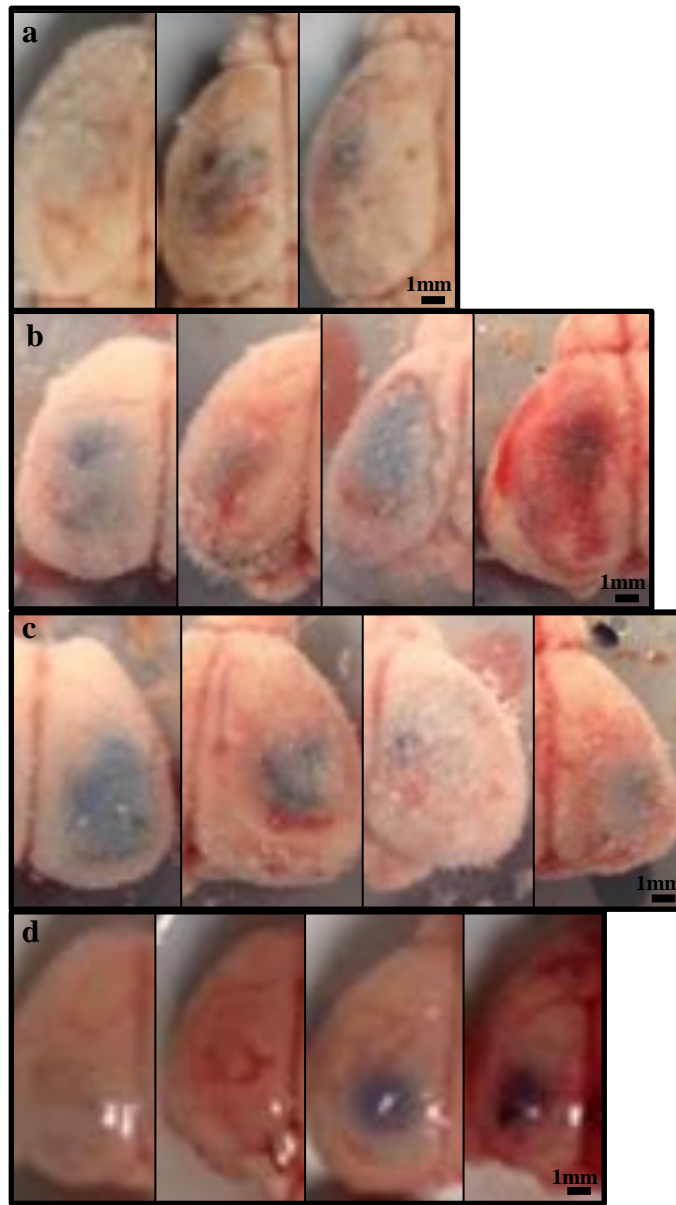


*Figure 9* Evans Blue dye transfer from single film implantations of 2% w/v thin silk films a) Transfer from films water-annealed for 1 hour implanted onto the dura of the left hemisphere of 3 brains b) Transfer from films water-annealed for 3 hours implanted onto the dura of the left hemisphere of 4 brains c) Transfer from films water-annealed for 4 hours implanted onto the dura of the right hemisphere of 4 brains d) Transfer from films water-annealed for 5 hours implanted onto the dura of the left hemisphere of 4 brains. Little to no transfer of dye was observed for all 2% w/v single films implantations.



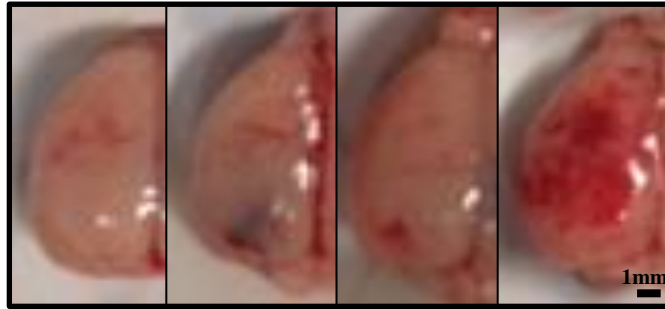


*Figure 10* Dye transfer from single film implantations of 5% w/v thin silk films water-annealed for 5 hours implanted onto the dura of the left hemisphere of 4 brains. Little to no transfer of dye was observed.

#### **4.1.2 Dual film implants**

Complications arising from implantation of single films in an in vivo environment led to the addition of a second film. These complications included the adhesion of the film and transfer of dye onto the underside of the bone flap. The second non-loaded film was produced from 5% w/v silk and water-annealed for 5 hours. The previous experiment using thin 2% w/v and 5% w/v dye-loaded films to determine the effect of water-annealing was repeated, but with the second film placed above the first dye-loaded film. The addition of the second non-loaded film was expected to prevent transfer of dye onto the underside of the bone flap and direct the dye through the dura of the brain. Figure 11 shows the results of dye transfer from 2% films water-annealed for 1, 2, 4, and 5 hours, and Figure 12 shows the results of dye transfer of 5% films water-annealed for 1 and 5 hours. Again, inconsistent transfer was observed despite the implantation of a second non-loaded film.

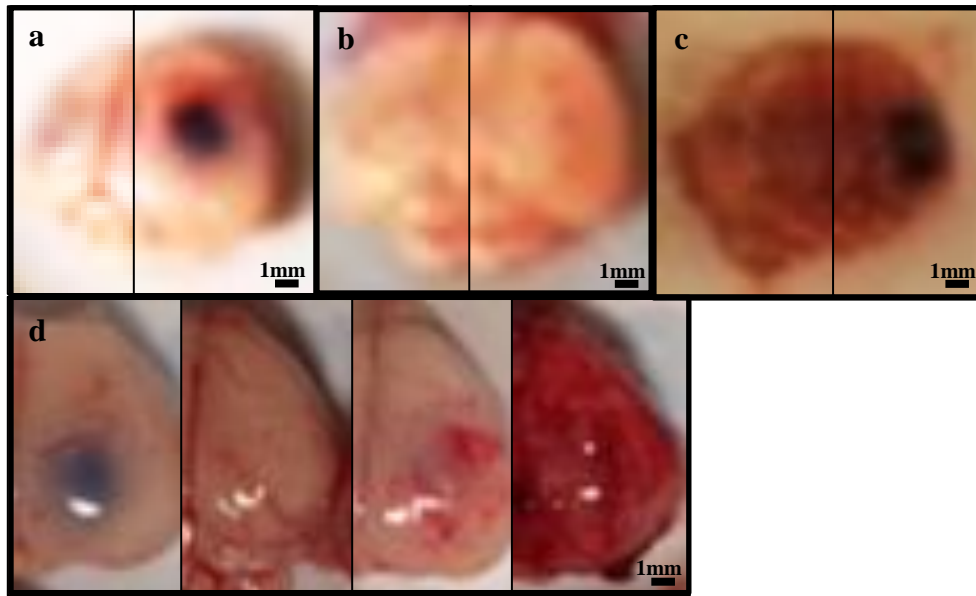


*Figure 11* Evans Blue dye transfer from dual film implantations where placement of a second 5% w/v non-loaded film followed implantation of a dye-loaded 2% w/v thin silk film a) Transfer from films water-annealed for 1 hour implanted onto the dura of the left and right hemisphere of 1 brain b) Transfer from films water-annealed for 2 hours implanted onto the dura of the left and right hemisphere of 1 brain c) Transfer from films water-annealed for 4 hours implanted onto the dura of the left and right hemisphere of 1 brain d) Transfer from film water-annealed for 5 hours implanted onto the dura of the right hemisphere of 4 brains. Little to no transfer of dye was observed for all dual film implantations.

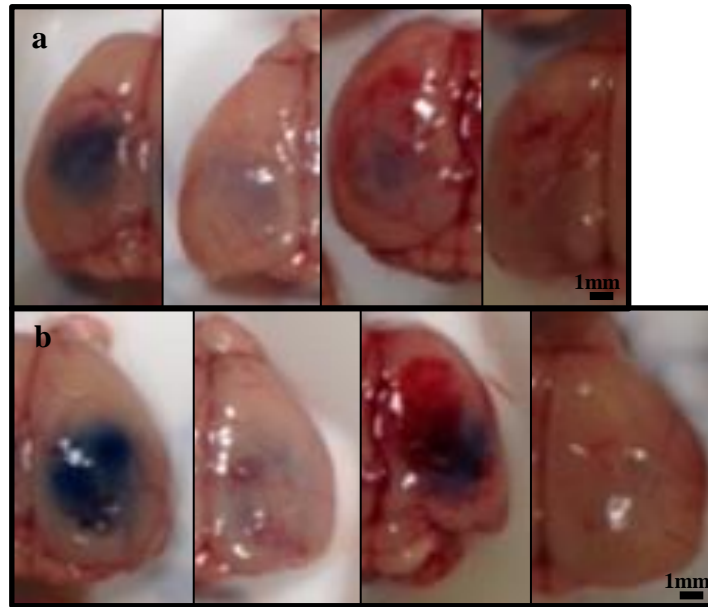
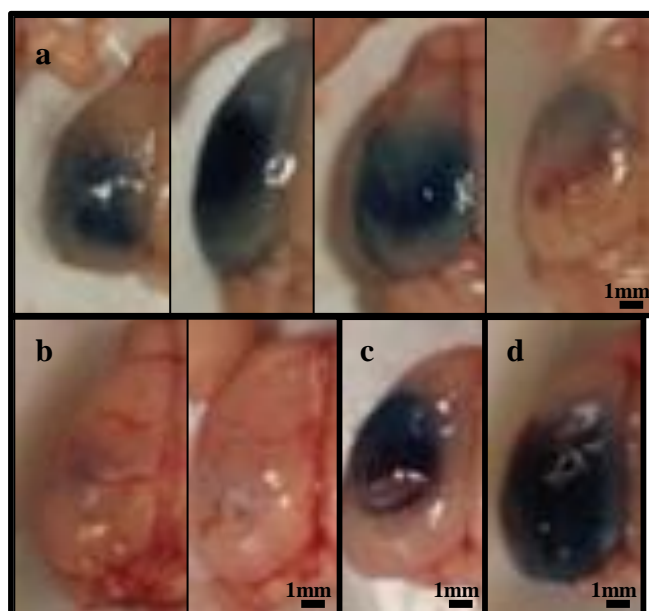


*Figure 12* Dye transfer from dual film implantations where placement of a second 5% w/v non-loaded film followed implantation of a dye-loaded 5% w/v thin silk film a) Transfer from films water-annealed for 1 hour implanted onto the dura of the left hemisphere of 4 brains b) Transfer from films water-annealed for 5 hours implanted onto the dura of the right hemisphere of 4 brains. Little to no transfer of dye was observed for all dual film implantations.

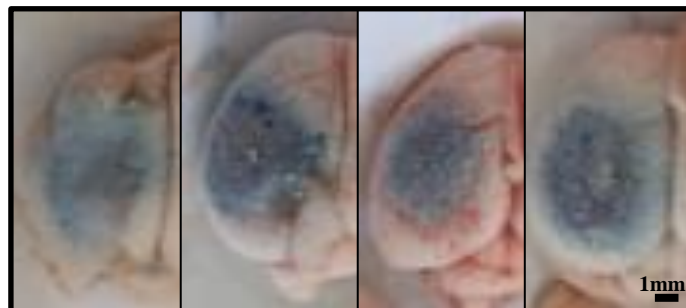
#### **4.1.3 Multiple dye-loaded film implants with adhesive**

The addition of a non-loaded film failed to prevent adhesion of the dye-loaded film to the underside of the bone flap. As a solution, multiple films were implanted with an adhesive (cyanoacrylate) sealing the bone flap to the skull for added pressure and to prevent the bone flap from lifting the films from the brain. Figure 13a shows the transfer of dye from 5% w/v silk films water-annealed for 1 hour after the adhesive was used to seal the bone flap at the surgical site. Significantly improved transfer was observed with some consistency. At the same time, the dose of dye delivered was increased either 2-fold or 3-fold to further promote the likelihood of consistent transfer to the dura. Figure 13c shows the

lack of transfer from implanting two dye-loaded films without an adhesive. Figure 13b depicts the necessity for an adhesive after two dye-loaded films were implanted with cyanoacrylate as no dye was observed. Figure 13d shows the transfer of dye from three dye-loaded films without adhesive, but implanting three separate films was difficult despite a large amount of dye on the dura. Figure 14 displays the consistent transfer of dye among 4 brains from implanting two-loaded films followed by the use of cyanoacrylate on the bone flap. This method of implantation became the preferred technique for delivering small molecules via thin silk films.



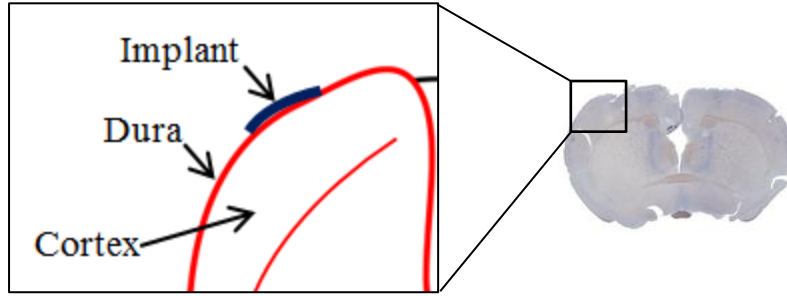
*Figure 13* Transfer of dye from 5% silk films water-annealed for 1 hour. a) Transfer of dye from a single film with the use of adhesive to seal the bone flap on the left hemisphere of 4 brains b) Transfer of dye from two dye-loaded films without an adhesive on the left hemisphere of 2 brains c) Transfer of dye from two-loaded films with the use of adhesive on the left hemisphere of 1 brain d) Transfer of dye from three dye-loaded films without an adhesive on the left hemisphere of 1 brain.



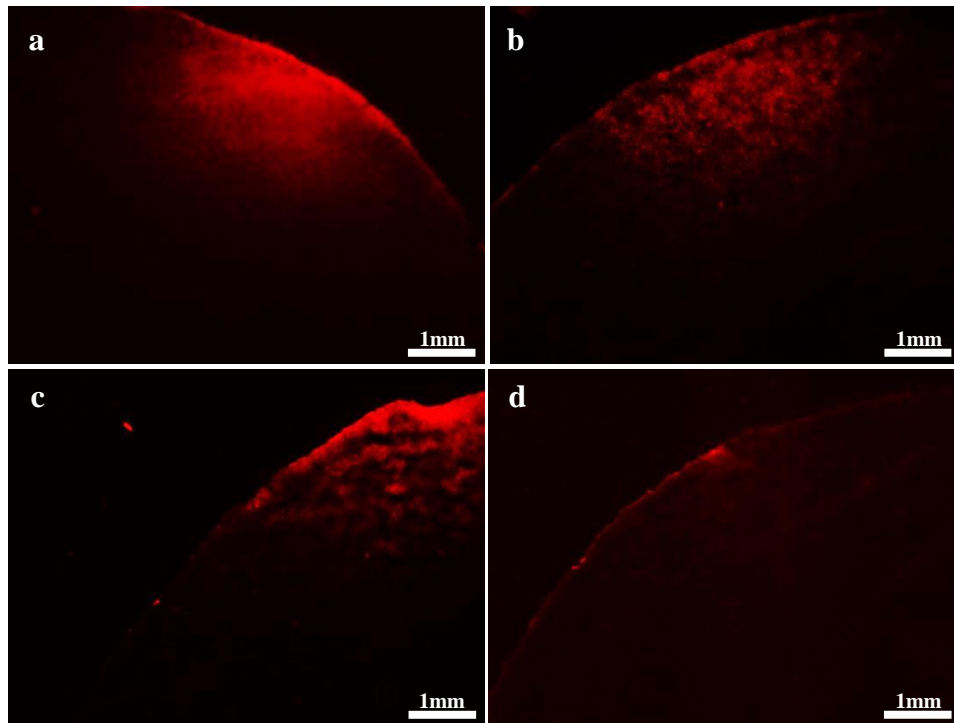
*Figure 14* Consistent transfer of dye from two dye-loaded films (5% w/v silk, water-annealed for 1 hour) with the use of an adhesive on the bone flap on the left hemisphere of 4 brains. Brains were frozen at the time the image was taken.

#### **4.1.4 Transcortical transfer of dye from thin silk film implants**

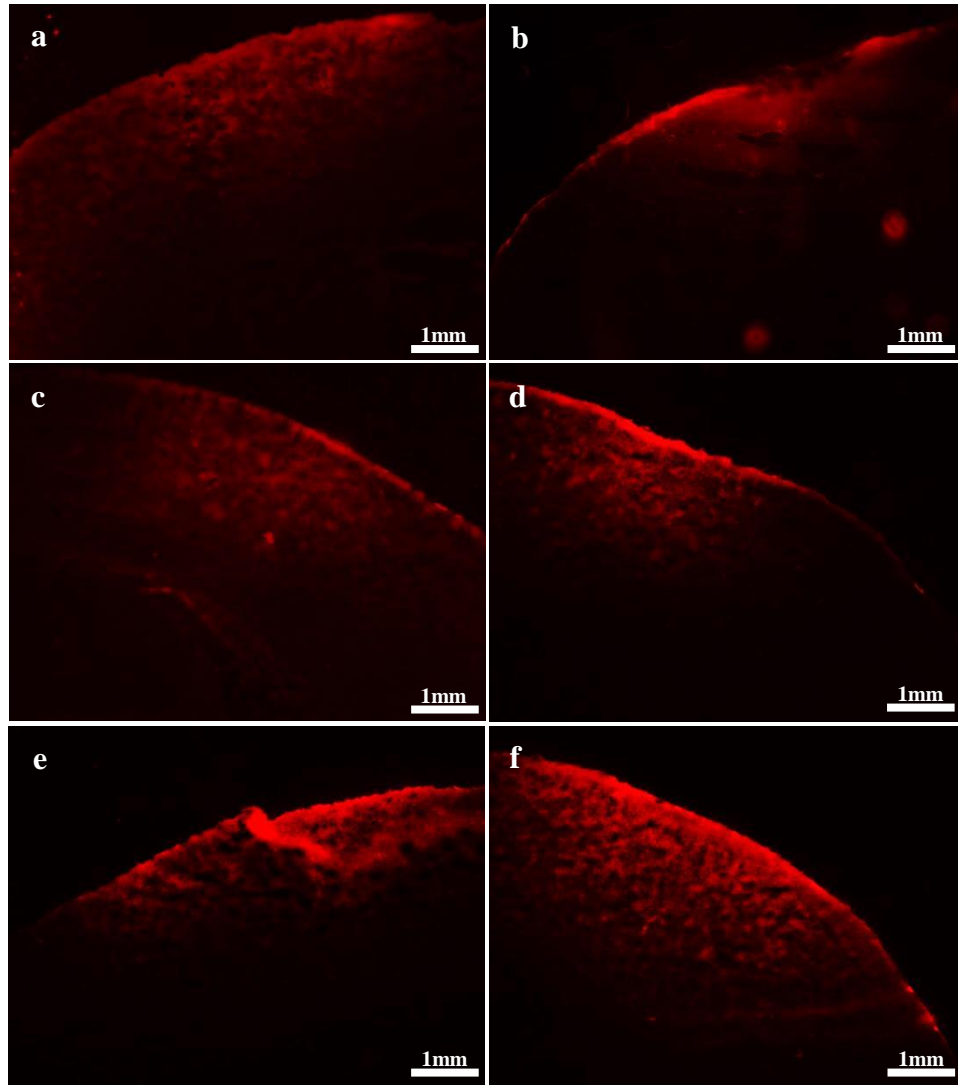
Figures 16-19 were captured under the CY3 filter of a Nikon Eclipse Ti fluorescent microscope. The images display transcortical transfer of Evans Blue dye from the films implanted in Figures 9-14. The goal was to observe consistent transfer of dye into the cortex in order to obtain maximum effects from small molecule delivery in the future. Figure 16 displays the transfer from single films which transferred dye poorly and inconsistently with any observed traces of dye either covering the surface of the dura or delivering to the outer perimeter just within the cortex. Figure 17 displays the transfer from dual film implantations. Similar degrees of penetration were observed along with inconsistent transfer which was a major flaw in the design of these implants.



*Figure 15* Schematic of film placement (left hemisphere) from the coronal view which correlates to transcortical transfer images (Figures 16-19 and 27). Only transfer of fluorescent dye is visible in the figures. (In some experiments, implants were also placed on the right hemisphere).



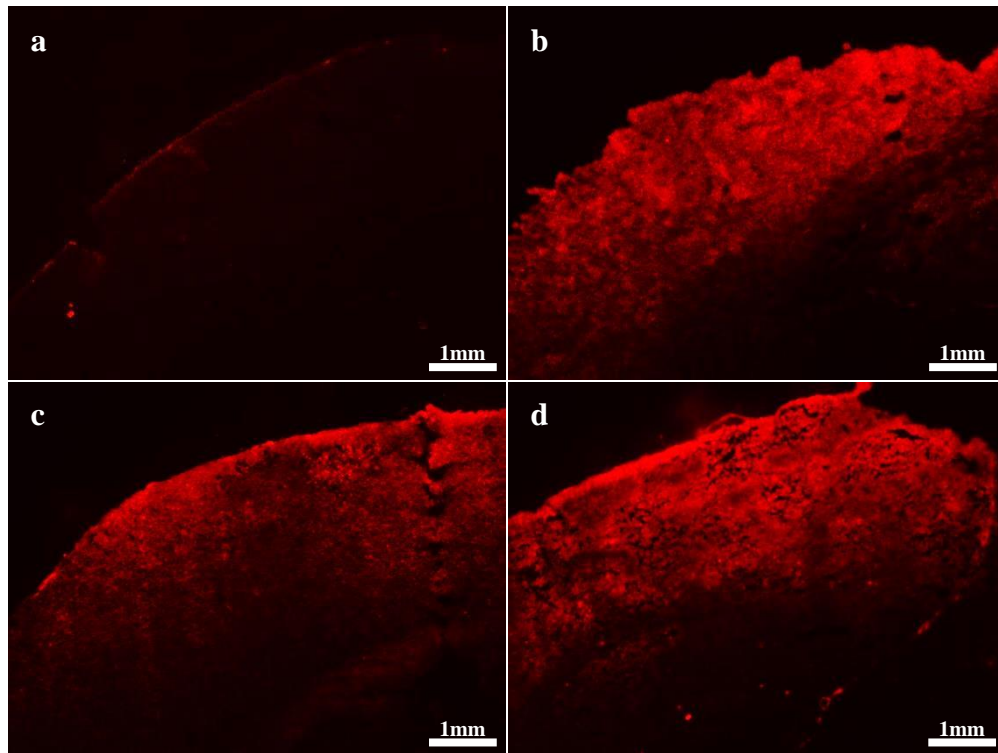
*Figure 16* Transcortical transfer of dye from single film implantations a) Transfer from a 2% film water-annealed for 3 hours b) Transfer from a 2% film water-annealed for 4 hours c) Transfer from a 2% film water-annealed for 5 hours d) Transfer from a 5% film water-annealed for 5 hours. Transfer for all films were either only on the surface of the dura or just within the outer perimeter of the cortex.



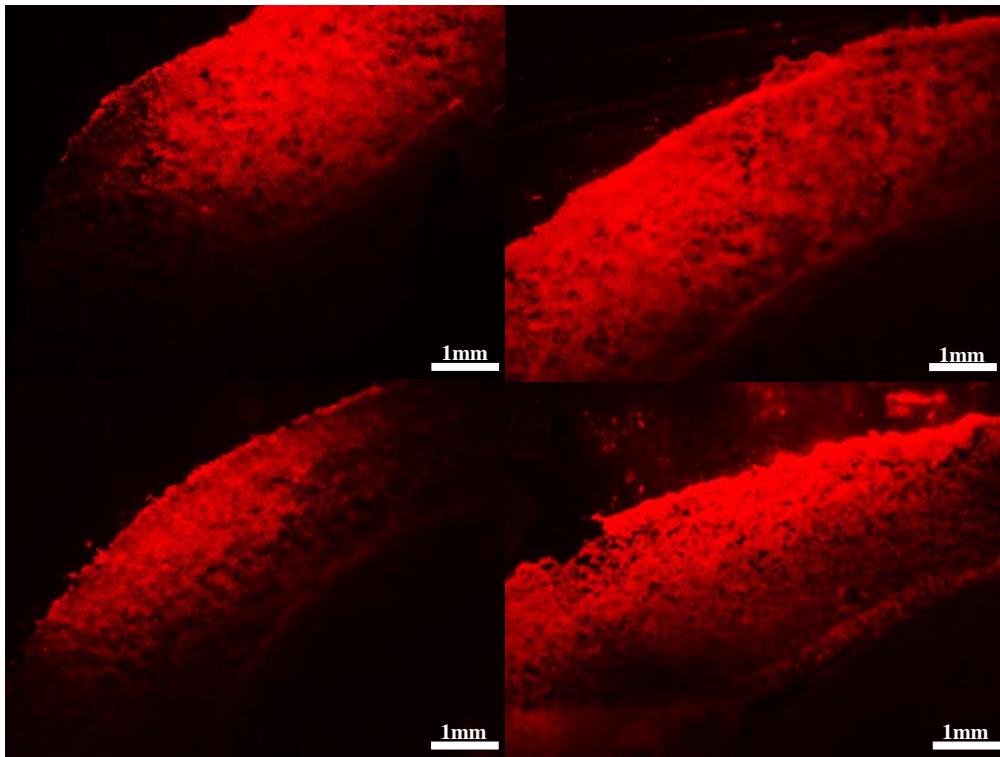
*Figure 17* Transcortical transfer of dye from dual film implantations where implantation of 5% silk film water-annealed for 5 hours was placed above a dye-loaded film a) Transfer from a 2% film water-annealed for 1 hour b) Transfer from a 2% film water-annealed for 2 hours c) Transfer from a 2% film water-annealed for 4 hours d) Transfer from a 2% film water-annealed for 5 hours. e) Transfer from a 5% film water-annealed for 1 hour f) Transfer from a 5% film water-annealed for 5 hours. Similar to single film implantations, transfer from all dual film implants did not consistently penetrate deep within the cortex.

Figure 18 displays the significantly improved transcortical transfer of dye with the application of an adhesive after implanting multiple dye-loaded films (5% w/v silk, water-annealed for 1 hour). Figure 18a displays the result from two dye-loaded films with no adhesive which released similarly to previous implantations without adhesive while Figure 18c is the same set of films sealed with an adhesive. There is complete transcortical transfer with this technique. Figure 18b displays the result of a single film sealed with an adhesive and Figure 18d shows the transfer of three dye-loaded films without an adhesive. Both sets of implantations showed successful delivery. However, inconsistent delivery was again a challenge with single films, and surgical complications prevented the ease of layering three separate films. Thus, the implantation technique from Figure 18c was repeated. The results are displayed in Figure 19 where all four brains showed consistently successful transcortical penetration of dye. This became the final technique for delivering small molecules with thin silk films.





*Figure 18* Transcortical transfer of dye from 5% silk films water-annealed for 1 hour  
a) Transfer from two dye-loaded films without the use of an adhesive b) Transfer from a single dye-loaded film with an adhesive c) Transfer from two dye-loaded films with an adhesive d) Transfer from three dye-loaded films without an adhesive. Penetration of dye within the cortex increased significantly with the application of an adhesive to the bone flap when compared to previous single and dual film implantations.



*Figure 19* Consistent transcortical delivery of dye in four mice from the final technique of thin silk film delivery (implantation of two dye-loaded 5% silk films water-annealed for 1 hour followed by the use of an adhesive on the bone flap)

#### **4.1.5 Small molecule delivery**

Two small molecules were loaded into thin silk films: propidium iodide (PI) and dizocilpine (MK801). PI, a cell death marker, was used to determine the success of MK801 in reducing the number of injured cells induced by controlled cortical impact (CCI). Before testing the release and effects of MK801, various doses of PI were loaded into films to determine which concentration was best for cell counts. Because two films were layered during implantation, the final dose delivered to each mouse was doubled. Figure 20 displays the release of PI at three different doses: a)  $0.125\mu\text{g}/\text{film}$  ( $0.25\mu\text{g}/\text{mouse}$ ) b)  $0.5\mu\text{g}/\text{film}$  ( $1.0\mu\text{g}/\text{mouse}$ ) c)  $0.875\mu\text{g}/\text{film}$  ( $1.75\mu\text{g}/\text{mouse}$ ). Each condition was implanted into one of three

mice. An appropriate increase in PI+ (injured cells) was observed as the concentration increased. Based on these results, a concentration between 1.0 $\mu$ g and 1.75 $\mu$ g per mouse was to be used for further small molecule experiments.

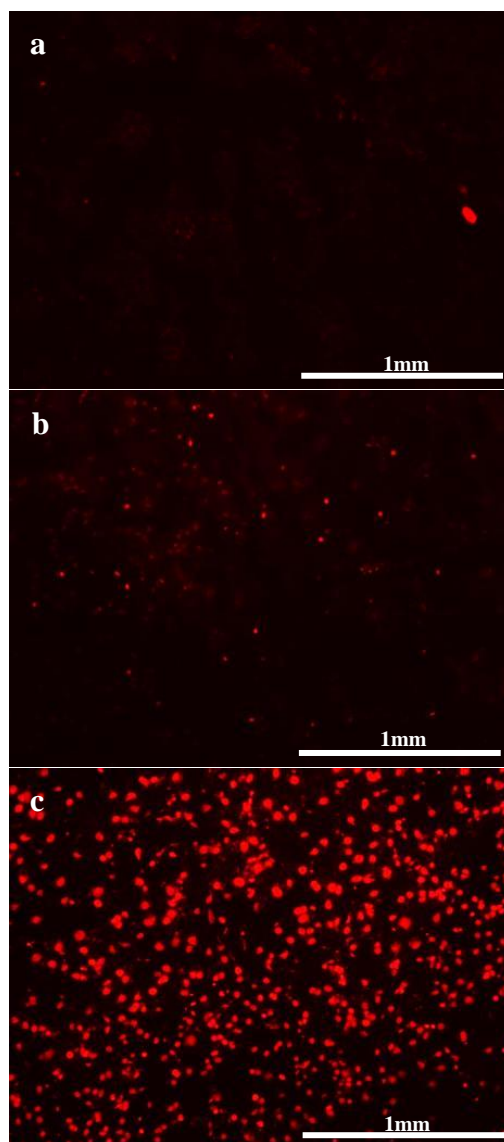


*Figure 20* Sections with increased doses of PI a) 0.125 $\mu$ g/film (0.25 $\mu$ g/mouse) b) 0.5 $\mu$ g/film (1.0 $\mu$ g/mouse) c) 0.875 $\mu$ g/film (1.75 $\mu$ g/mouse). PI+ (injured) cells are indicated by the red fluorescent cells. The extent of injury is the same in all three images, but higher doses of PI were able to mark a greater number of injured cells.

Figure 21 displays the results from loading MK801 into thin silk films. PI was delivered to each mouse at a concentration of  $0.75\mu\text{g}/\text{film}$  ( $1.5\mu\text{g}/\text{mouse}$ ). MK801 was also incorporated into two sets of implants at a concentration of  $15\mu\text{g}/\text{film}$  ( $30\mu\text{g}/\text{mouse}$ ). Figures 21a and 21b display sections from control mice where films only delivered PI before performing CCI. Figures 21c and 21d display the result from the addition of MK801 to the films. There was inconsistency in the amount of PI that penetrated the control mice which made determining the success of MK801 on injured brains inconclusive.

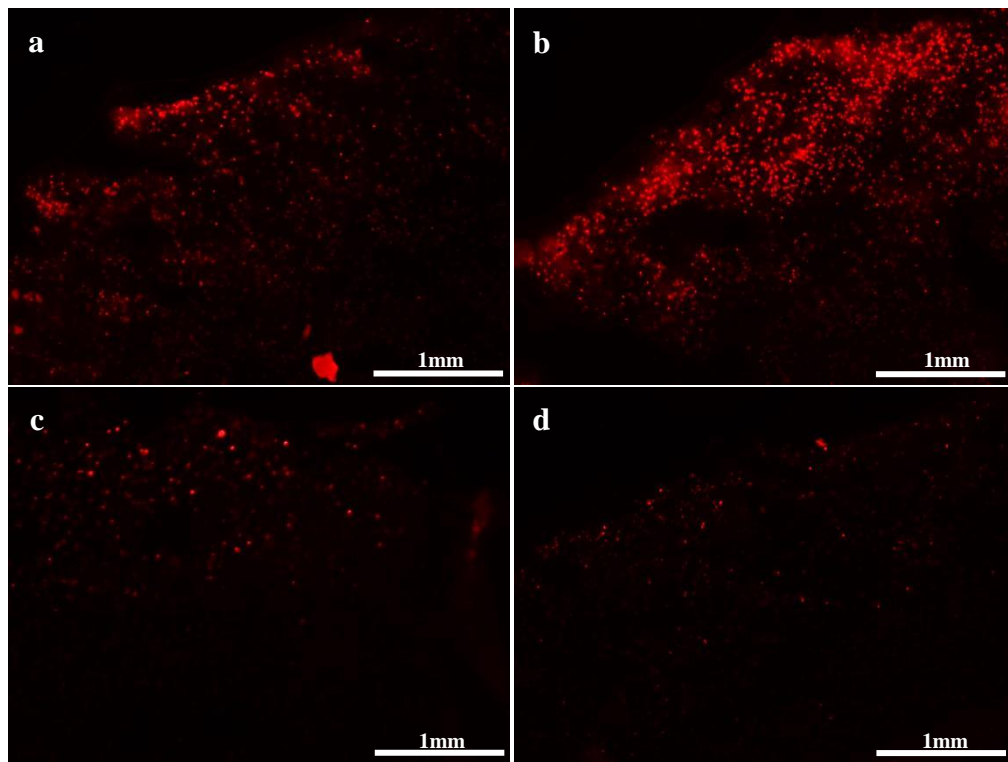


*Figure 21* Sections from films loaded with PI and MK801 a) & b) Controls with only PI c) & d). Sections treated with MK801. Inconsistency in control films provided inconclusive results on the effects of MK801 following CCI.

## 4.2 Discussion

The effects of water-annealing on the solubility of thin silk films in addition to the release of small molecule dyes from silk films have been extensively studied in vitro [54, 55, 56]. Thus, the next step was to observe these trends in vivo through the application of treating TBI via localized small molecule delivery. Silk films with a concentration of 2% w/v were expected to contour to the brain increasing the contact surface area from which films would be able to maximize drug delivery. Based on previous research, increasing water-annealing time slows the rate at which films dissolve and thus the rate at which small molecules release. Observing the release of Evans Blue dye from thin silk films implanted directly onto the dura would help determine which water-annealing time produced films that had minimal burst release and maximum dye transfer following 24 hours aligning with the selected CCI mouse model. Figure 9 displays the results of increasing water-annealing time on the transfer of dye. Unfortunately, neither low nor high anneal times produced successful consistent transfer with all four times displaying little to no transfer. The reason for these results was most likely due to a burst release from all films and the clearance of dye by CSF soon after implantation. As a solution, slightly thicker films were casted as they were expected to have a slower release. Thicker films were made by increasing the silk concentration to 5% w/v, and because of the increased concentration, a higher anneal time was chosen to induce beta-sheet formation. Figure 10 displays the results of these films annealed for 5 hours. Again, there were inconsistent results with little to no transfer. However, these films remained intact following 24 hours

and were found adhering to the underside of the bone flap to where much of the dye had transferred. This observation suggested that these films were transferring dye onto the skull rather than onto the surface of the brain. To resolve this complication, dual film implantations were performed. Following the implantation of a dye-loaded film, a non-loaded film (5% w/v, annealed for 5 hours) was placed to prevent transfer onto the underside of the skull and force transfer onto the dura. The initial experiment of determining the effect of water-annealing time in vivo was repeated with the dual film implantation approach. Figures 11 and 12 display the results from 2% and 5% films, respectively. Brains that showed transfer showed a greater amount of dye than single film implantation, but the results were not consistent. The 5% silk films again remained intact and adhered to the underside of the skull signifying that poor transfer was most likely due to lack of contact with the surface of the brain rather than transfer to the underside of the bone flap. For the next round of implantations, rather than adjusting the properties of the films, the implantation technique was modified. Following implantation and the replacement of the bone flap, an adhesive was used to seal the skull and apply a slight amount of pressure. This modification was expected to minimize the gap between the bone flap and the dura and increase the contact of the film with the brain. In addition to applying an adhesive, the dose was also increased but implanting multiple dye-loaded films to determine if an increase in dye concentration was required to observe consistent results. Figure 13 displays the results of applying an adhesive and implanting two and three dye-loaded films. The transfer of dye increased

significantly with the applied pressure from the adhesive as can be seen when comparing Figures 13b and 13c where two dye-loaded films were implanted without and with an adhesive. Figure 13a displays improved results, but with some inconsistency by implanting only a single film with adhesive. Lastly, Figure 13d shows the transfer from three dye-loaded films without adhesive. Despite significant transfer, the implantation of three separate films was difficult. Based on the results of this last experiment to determine effective film design and implantation technique, the preferred method for future small molecule release from thin silk films was with two drug-loaded films with the application of an adhesive on the bone flap. To ensure consistency of this approach, a subsequent round of implantations practicing this technique was performed and the results are seen in Figure 14 where all four brains showed consistent dye transfer.

In order to confirm delivery of dye into the cortex not solely on the surface of the dura, the depth of transcortical transfer was observed under a fluorescent microscope. Figures 16 and 17 display the transcortical transfer from single and dual film implantations, and Figures 18 and 19 display the transfer from implantations with adhesive and multiple films. The depth of transfer from these films was consistent with the transfer of dye onto the dura. The films that displayed transfer onto the dura showed fluorescence within the cortex. However, the main problem from these films was consistency. Additionally, complete transcortical delivery is crucial in order to have the greatest effect from further small molecule delivery. The implantations that showed the greatest dural

transfer, from films with adhesive and multiple dye-loaded films, displayed significant transcortical delivery of dye. Figure 18 shows significant fluorescence throughout the cortex, with the exception of Figure 18a which shows transfer from two dye-loaded films implanted without adhesive. This enforces the necessity of an adhesive on the bone flap. Figure 19 displays the consistency of transcortical transfer from the implantation technique of choice for future small molecule delivery experiments: two drug-loaded films implanted with the application of adhesive on the bone flap. Although these films produced consistent delivery, the films remained intact following 24 hours. However, consistency of delivery was a higher priority than drug loss in order to produce viable quantitative results.

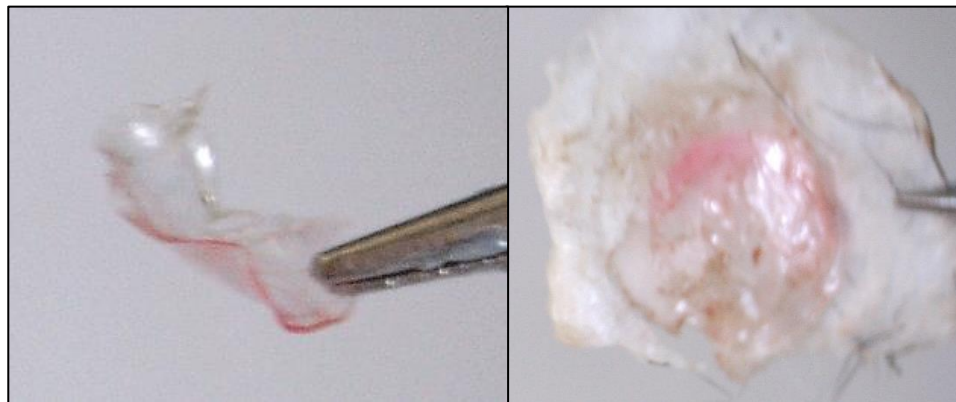
Small molecule experiments began with determining the dose of PI from which injured cell counts could be measured. Unlike prior dye-loaded film experiments, CCI was performed following film implantation during small molecule experiments. Figure 20 displays the results from films loaded with three different doses of PI: a) 0.25 $\mu$ g b) 1.0 $\mu$ g c) 1.75 $\mu$ g. With the increase in PI, an increased number of injured cells were observed as expected. For further experiments, a dose of PI equal to 1.5 $\mu$ g was used for injured cell counts as higher doses saturated the injured area.

The first therapeutic small molecule tested was dizocilpine (MK801), an NMDA antagonist. A dose of 30 $\mu$ g delivered to each mouse along with 1.5 $\mu$ g of PI.

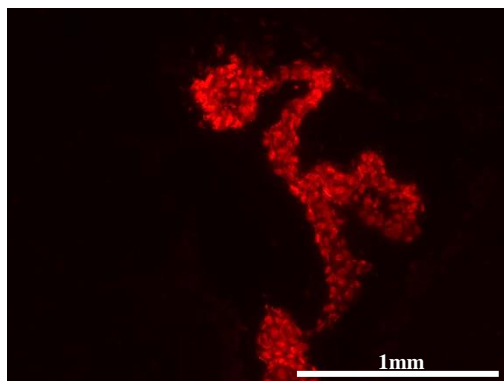


Figure 20 displays the results of MK801 delivery where Figures 21a and 21b are sections from control mice and Figures 21c and 21d are from sections treated with MK801. Unfortunately, the effect of MK801 was inconclusive because the delivery of PI to the controls was inconsistent. With varying degrees of PI+ cells in the control, whether or not MK801 had a therapeutic effect and reduced the number of injured cells following CCI was indeterminate.

As mentioned previously, the current film design and implantation procedure resulted with intact films after 24 hours. Figure 22 displays post-implantation films loaded with PI. Variations in delivery were most likely due to the extent to which films dissolved and consequently released small molecules. In this particular in vivo environment, CSF is responsible for dissolving films which was supported by the appearance of PI in the choroid plexus (Figure 23), the area of the brain that produces and circulates CSF. To address this problem, drug delivery from silk-HRP hydrogels were explored as an alternative with greater potential for consistent results.



*Figure 22* Intact post-implantation films loaded with PI



*Figure 23 PI delivery via CSF to the choroid plexus*

## **5. Silk-HRP Hydrogels**

### **5.1 In vitro results**

Silk-HRP hydrogels were loaded with 100 $\mu$ g of Evans Blue dye and maintained a 5% w/v silk concentration. The release of dye from hydrogels of different thicknesses, controlled by the total volume of silk-HRP solution, was observed over a drop of 100 $\mu$ L of water (Figure 24). The thicker hydrogels took a longer time to release dye as expected. Figure 25 shows the release kinetics of dye from the same hydrogels over the course of 24 hours. Again, as expected, the thicker hydrogels displayed a slower release when compared to thinner hydrogels. These results were used to determine which hydrogels were to be implanted in vivo in order to minimize burst release.

### 5.1.1 Hydrogel release

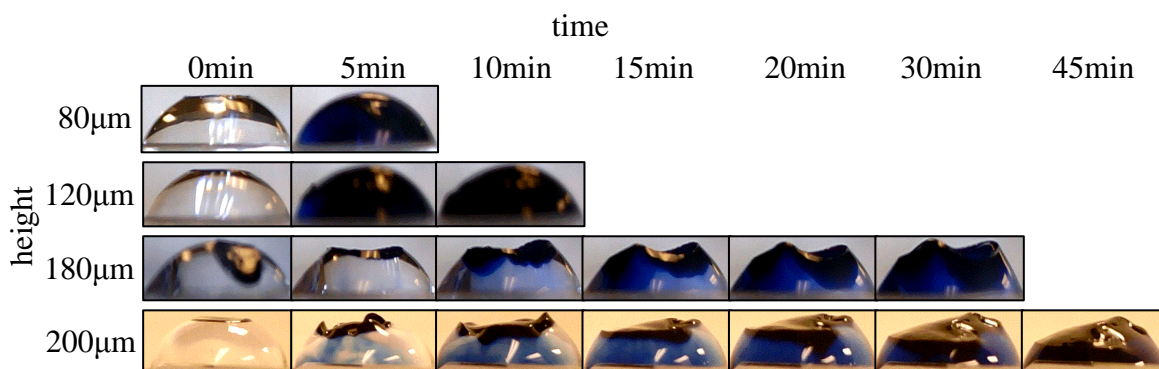


Figure 24 Dye release from hydrogels with different heights

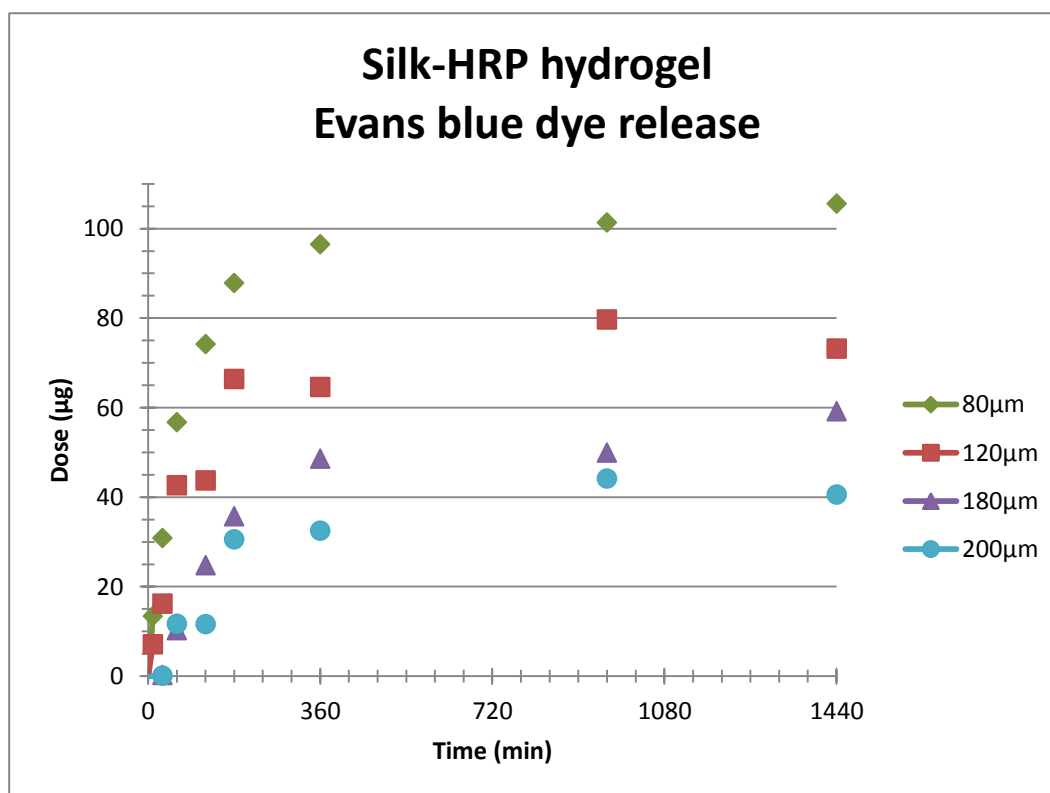
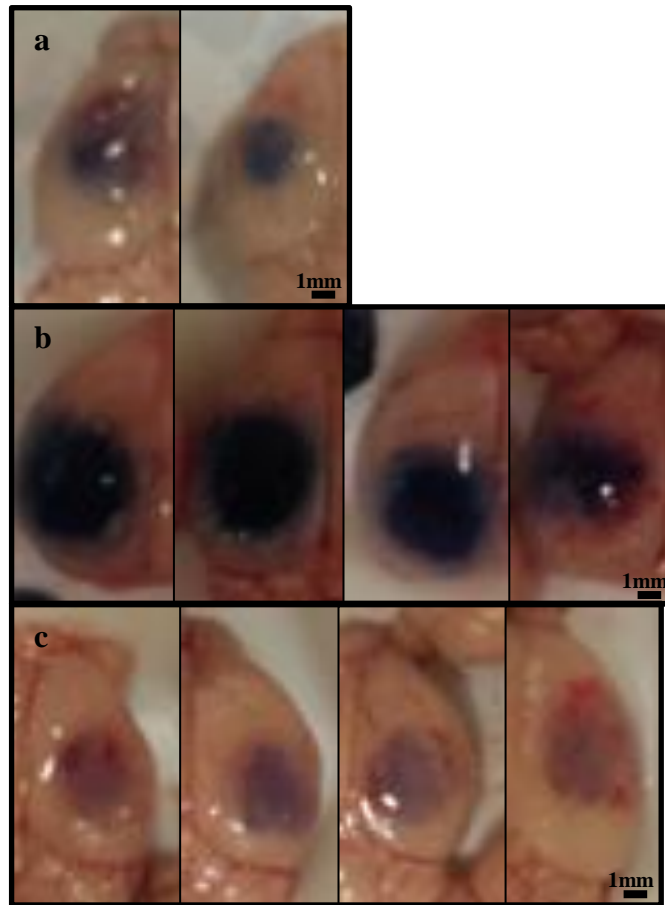


Figure 25 Evans Blue dye release from hydrogels of different heights over 24 hours

## **5.2 In vivo results**

### **5.2.1 Silk-HRP hydrogel implants**

Silk-HRP hydrogels with heights of 120 $\mu$ m and 180 $\mu$ m were chosen to be implanted based on the previous in vitro results. The goal was to determine which hydrogels would transfer dye to the dura and cortex consistently. Both hydrogels showed consistent delivery with the 180 $\mu$ m-thick hydrogels displaying greater transfer. Release time was also studied when comparing release of 180 $\mu$ m-thick hydrogels after 24 hours and after 6 hours. After 6 hours, brains showed poor transfer, and as a result, continuing experiments with silk-HRP hydrogels were conducted using 180 $\mu$ m-thick hydrogels releasing over 24 hours (Figure 26).



*Figure 26* a) Hydrogels approximately 120 $\mu$ m thick implanted on the left hemisphere of two brains for 24 hours b) Hydrogels approximately 180 $\mu$ m thick implanted on the left hemisphere of four brains for 24 hours c) Hydrogels approximately 180 $\mu$ m thick implanted on the left hemisphere of four brains for 6 hours. All hydrogels showed consistent transfer and the 180 $\mu$ m hydrogels showed the greatest transfer of dye.

### **5.2.2 Transcortical transfer of dye from silk-HRP hydrogels**

Figure 27 was captured under the CY3 filter of a Nikon Eclipse Ti fluorescent microscope. The image displays transcortical transfer of Evans Blue dye from hydrogels implanted in Figure 27. The goal, as with the films, was to observe consistent transfer of dye into the cortex in order to obtain maximum effects from small molecule delivery in the future. Figure 27a displays the depth of transfer from a 120 $\mu$ m-thick hydrogel and Figure 27b displays the depth of transfer from a 180 $\mu$ m-thick hydrogel both after 24 hours. Figure 27c is also the result from a 180 $\mu$ m-thick hydrogel, but after a release of 6 hours. All showed consistent transfer with the 180 $\mu$ m-thick hydrogels after 24 hours showing greater fluorescence and therefore greater delivery.

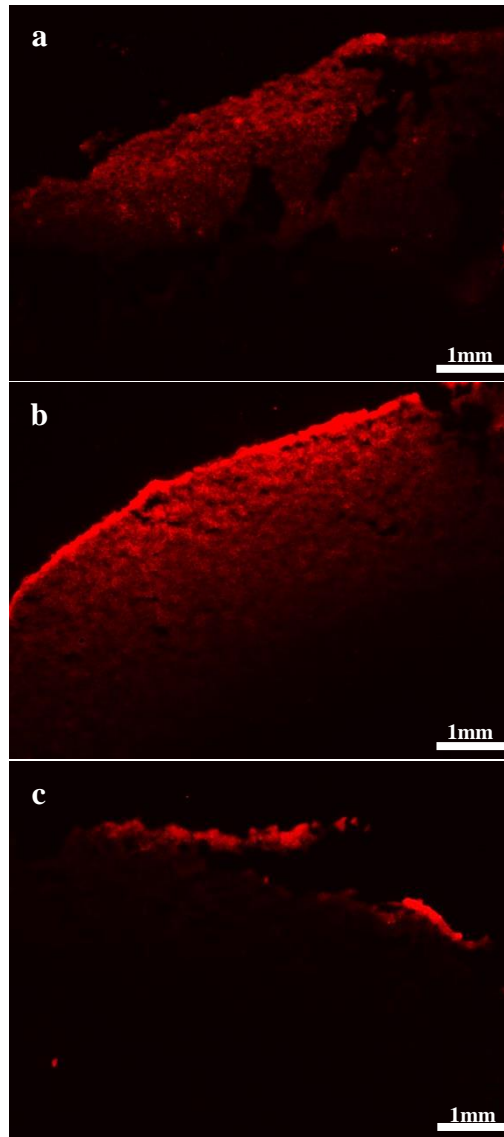


*Figure 27* a) Slight transcortical transfer of dye from a 120 $\mu$ m-thick hydrogel after 24 hours b) Strong transcortical transfer of dye from a 180 $\mu$ m-thick hydrogel after 24 hours c) Poor transcortical transfer of dye from a 180 $\mu$ m-thick hydrogel after 6 hours. Hydrogels releasing dye for 24 hours showed greater depth of transfer with the 180 $\mu$ m thick hydrogels providing the optimal result.

### 5.2.3 Small molecule delivery

Two small molecules were loaded into silk-HRP hydrogels: PI and glutathione (GSH). Again, PI was used to determine the success of GSH in reducing the number of injured cells induced by CCI. Additionally, Evans Blue dye was loaded into the hydrogels to better visualize delivery onto the dura. PI was loaded at a concentration of  $1.5\mu\text{g}/\text{hydrogel}$ , GSH was loaded at a concentration of  $100\mu\text{g}/\text{hydrogel}$ , and dye was loaded at a concentration of  $100\mu\text{g}/\text{hydrogel}$ . Figure 28 displays the results of GSH delivery where Figure 28a is a section from the control with only PI and dye and Figure 28b is a section treated with GSH. The results of this experiment were inconclusive as the background fluorescence from the dye prevented accurate PI+ cell counts.

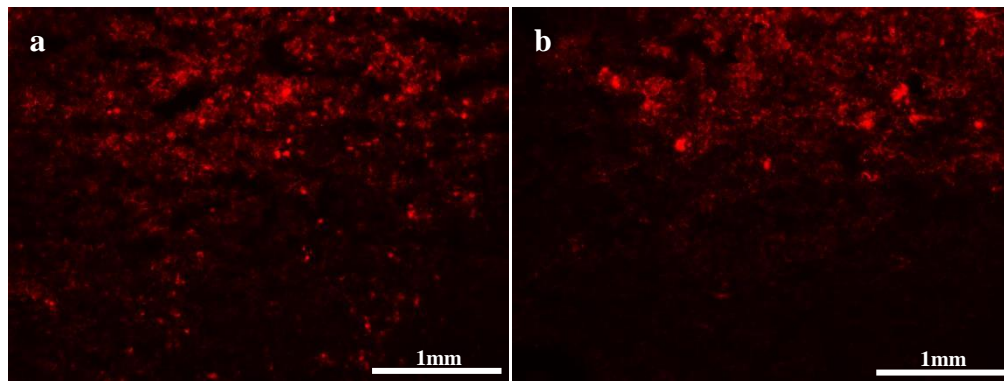


*Figure 28* Sections from PI, GSH and dye delivery a) Section from control with only PI and dye b) Section with the addition of GSH.



Figure 29 displays the result of hydrogels loaded with GSH (100 $\mu$ g/hydrogel) and a reduced concentration of dye (50 $\mu$ g/hydrogel). During this experiment rather than loading PI into the hydrogels, it was administered via an intraperitoneal injection (30mg/mouse) immediately following CCI. Figures 29a and 29b are sections from the control mice whereas Figures 29c and 29d are sections from mice treated with GSH. Unfortunately, through qualitative observation, there was no significant difference between the control and treatment with GSH.

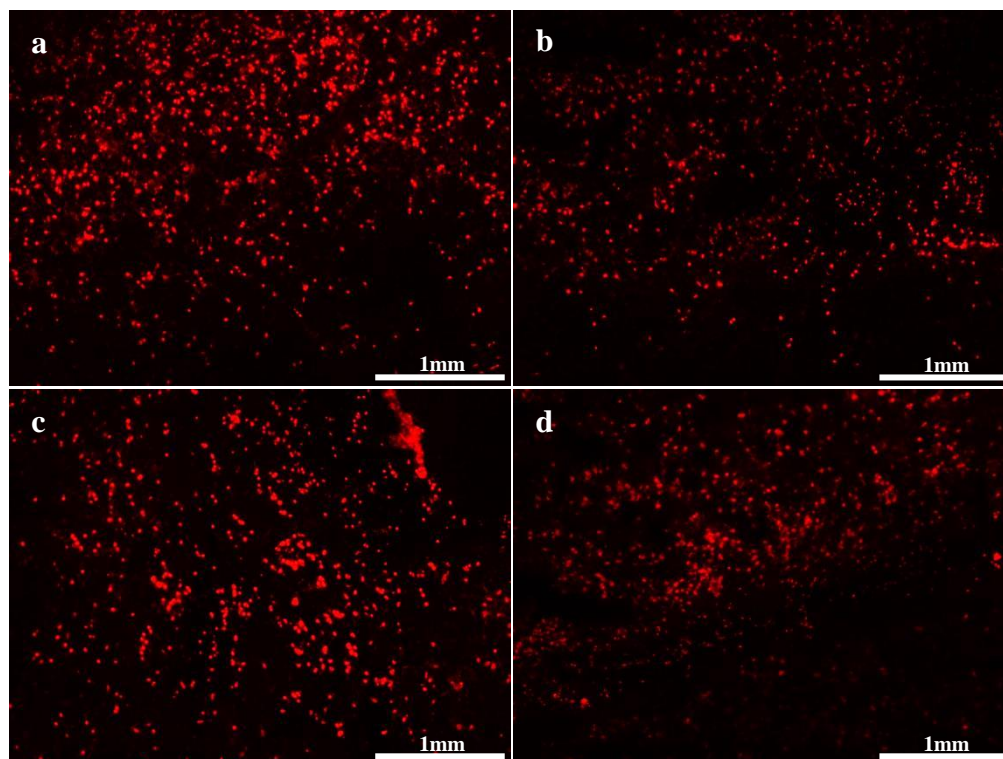


*Figure 29* Sections from GSH and dye delivery with intraperitoneal injection of PI a) & b) Control sections treated with hydrogels loaded with dye only c) & d) Sections treated with hydrogels loaded with dye and GSH.

### 5.3 Discussion

Silk-based hydrogels have previously been used as scaffolds for brain tissue regeneration [57]. However, limited research has been done on silk-HRP hydrogels for localized drug delivery to treat traumatic brain injury. In this project, hydrogels were implanted when thin silk films posed complications with obtaining consistent small molecule release due to CSF circulation. Whereas release from silk films requires fluid to dissolve films, silk-HRP hydrogels release via diffusion and may remain intact once release has finished. With respect to this research, if hydrogels remained intact following 24 hours, consistent release was still possible. However, the relationship between CSF clearance and drug release is unclear and has the potential to yield similar consistency complications.

Silk-HRP hydrogel design was first tested in vitro via Evans Blue dye release. Hydrogels of increasing thicknesses were loaded with 100 $\mu$ g of dye and casted with the expectation that thicker hydrogels decreased the rate of release. Figure 24 depicts the diffusion of dye when hydrogels are exposed to 100 $\mu$ L of water. As expected, thicker hydrogels took longer to release dye. To quantify the release, silk-HRP hydrogels were immersed in 1X PBS for a duration of 24 hours. Hydrogels 80 $\mu$ m in height released all 100 $\mu$ g of dye within 24 hours while hydrogels 200 $\mu$ m in height released on average 40% of dye over 24 hours (Figure 25).

To test dye release in vivo, both 120 $\mu$ m- and 180 $\mu$ m-thick hydrogels were implanted, and the results are depicted in Figure 26. Both implants were released over 24 hours with both hydrogels remaining intact. The 180 $\mu$ m-thick hydrogels had a significantly greater amount of transfer onto the dura when compared to the 120 $\mu$ m-thick hydrogels although both had consistent results. The 180 $\mu$ m-thick hydrogels were also implanted to observe a 6 hour release, but transfer was light although again consistent across all four brains. The observations made from silk-HRP hydrogel implantations indicate they are more effective and consistent compared to thin silk films. When implanting two dye-loaded films, 200 $\mu$ g of dye was delivered (100 $\mu$ g/film) whereas loading 100 $\mu$ g in one hydrogel implant produced the same if not greater transfer. Additionally, regardless of the height of the gel and their respective release of dye, the results were consistent, a major disadvantage of implanting films.

Transcortical transfer was also observed and the results are depicted in Figure 27. Based on the fluorescence, the implant with the most potential for successful small molecule delivery was a hydrogel with a height of 180 $\mu$ m released over 24 hours.

Small molecule experiments with silk-HRP hydrogels began with glutathione (GSH), an antioxidant. Unlike film implants, hydrogels were also loaded with dye to visualize the transfer onto the dura and ensure delivery into the cortex prior to sectioning. Figure 27 displays the results from this experiment. PI+ cells were

identified in both mice. However, background fluorescence from the dye made obtaining accurate PI+ cell counts difficult. Thus, in the following experiment, the dose of dye was reduced by 50%. PI was also administered via an IP injection rather than through hydrogel release. The dose of GSH loaded into the hydrogel remained the same. The results are displayed in Figure 29. Initial qualitative observations indicate that GSH, at this dose, did not significantly reduce the number of injured cells following CCI.

The silk-HRP hydrogels which remained intact following 24 hours in this experiment are depicted in Figure 30. Following removal, hydrogels shrunk with exposure to air. Unlike film implants, obtaining consistent results from small molecule delivery has not appeared to be problematic thus far.

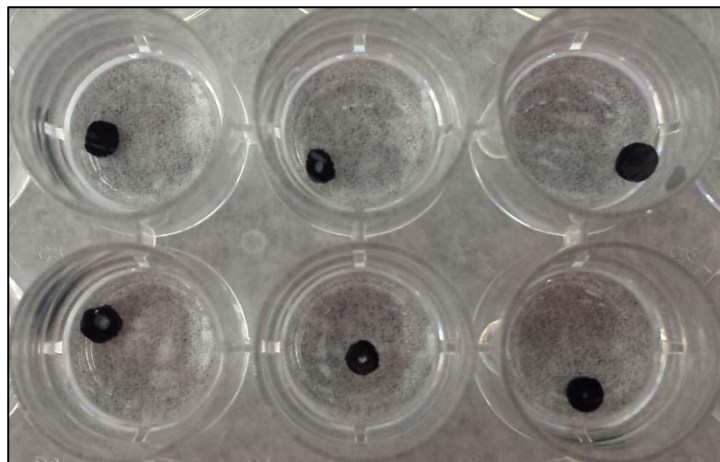


*Figure 30* Intact post-implantation hydrogels

## 6. Conclusion

The main objectives of this project were to design an implant to consistently deliver small molecules to the brain over the course of 24 hours and to determine the effects of these drugs on injured tissue following a CCI mouse model. The first objective was initially addressed with thin silk films and because of the inability to generate consistent results, silk-HRP hydrogels became the next implant of choice. Overall, hydrogels boast a greater advantage over films not only because of their capability to release consistently regardless of its height. As observed in dye experiments, to obtain the same transcortical transfer, films required twice the dose of dye as did hydrogels. This decreases the chances of inducing toxic side effects in further small molecule dosage experiments. Additionally, hydrogels had minimal burst release upon implantation unlike the films. As previously mentioned, the diffusion of small molecules into the cortex must be greater than the clearance rate of CSF, and this was not the case with the implantation of films. Because of their burst release, drugs were not able to diffuse into the cortex before being cleared by CSF. The effect of small molecules on injured tissue once released from silk implants was also briefly studied. Due to inconsistency in MK801 experiments, a therapeutic effect was indeterminate. However, MK801 has yet to be released from hydrogels. The effect of GSH on injured tissue appeared to have no effect at the selected dose. Future experiments with this molecule would include increasing its dose in addition to combining it with other small molecules for a combination release.

The two silk implants studied in this project different greatly in their ability to yield consistent results in a physiological environment. The design of thin silk films was manipulated by altering silk concentration and water-annealing time. Although previous work has shown the effect of these parameters on small molecule release, the same results were not observed *in vivo*. Rather, inconsistent delivery was observed making films an impractical implant of choice for the application of neural drug delivery. The design of silk-HRP hydrogels was manipulated by altering hydrogel height. *In vivo* delivery was comparable to *in vitro* release trends, but more importantly, delivery was consistent among implantations of the same hydrogel design. The consistency allows for experiments with small molecule drugs to produce quantifiable data and to potentially discover therapeutic drugs for TBI with statistically significant results.

## **6.1 Future Directions**

### **6.1.1 Quantify *in vitro* release of small molecule drugs**

The first objective of the next segment of this research project is to quantify the release of small molecule drugs *in vitro*. The small molecules tested *in vivo*, propidium iodide (PI), dizocilpine (MK801), and glutathione (GSH), were expected to release from silk-HRP hydrogels with similar kinetics as the Evans Blue dye used to test different implant designs (Figure 25). However, because of the differences in chemical structure, charge, and other properties, their interaction with hydrogels may differ than that with dye. Preliminary research conducted during this project supports these differences where MK801 release

from hydrogels indicates a faster release rate than dye. While significant transfer of dye onto the dura and into the cortex required 24 hours, release of MK801, at a dose of 30 $\mu$ g/hydrogel, displayed a functional outcome within one hour suggesting a higher release rate. Following one hour from hydrogel implantation, mice treated with MK801 became hyperactive and control mice showed no effect. The functional differences indicate the release of MK801 is faster than the release of dye and therefore both vary in their interaction with silk-HRP hydrogels. To quantify the release of small molecules in vitro, several methods may be considered. PI is a fluorescent molecule (excitation = 493nm) and thus UV-Vis spectroscopy can be used to detect the release of PI in 1x PBS in a well-plate. Absorbance values can then be compared against a standard release curve of PI to quantify approximate doses released from hydrogels. MK801 can be detected with the [3H](+)MK801 radioligand binding assay for which the protocol can be found in a previously published paper [58]. Lastly, the release of GSH from hydrogels can be screened for in vitro with the GSH detection kit from Enzo Life Sciences, Inc (Farmingdale, NY, USA). The quantification of other small molecule drugs will vary depending on the type of drug. Based on the functional outcomes observed in vivo from the delivery of MK801, the release kinetics of other small molecule drugs in vitro are expected to vary compared to the release kinetics of Evans Blue dye. Consequently, dye cannot be used to predict the successful delivery of other small molecule drugs from silk-HRP hydrogels.

### **6.1.2 Quantify in vivo release of small molecule drugs**

The quantification of small molecule drug release in vivo will determine statistical significance of their therapeutic effect, a crucial step in the process of drug discovery. Initial implant designs in this project were tested with qualitative observation of the transfer of Evans Blue dye onto the dura and into the cortex with fluorescence microscopy. Additional implant designs modified to account for the different chemical properties of other small molecule drugs should quantify the release of Evans Blue dye in initial in vivo release experiments. Quantification can be accomplished by measuring the area of transfer into the cortex and the intensity of fluorescence with Image J. To reach the goal of consistent transfer, results are expected to show little variation in area of transfer and intensity of fluorescence before continuing with the delivery of small molecules. The effect of drugs on decreasing cell death in this project was determined qualitatively. However, with large sample sizes cell death counts can be determined with PI. In the last experiment, PI was delivered via an IP (intraperitoneal) injection. Counting the number of injured cells, or cells marked with PI, in both control and treated tissue sections will help determine their statistical significance on decreasing cell death. After ensuring the release of drugs from silk-HRP hydrogels in vitro, treated samples are expected to show a decrease in the number of injured cells.



### **6.1.3 Determine effect of delivery pre- and post-injury**

Unfortunately, several preclinical studies examine drug release outside therapeutic windows relevant to humans. In most cases, animal models employ a pre-treatment paradigm where drugs are delivered pre-injury posing a non-realistic scenario. When drugs are delivered post-injury, they are delivered very early, usually in less than one hour following injury. These time points do not correlate to the actual treatment of TBI patients where factors such as informed consent must be considered prolonging the administration of drugs. Additionally, pharmacokinetic and pharmacodynamic profiles are difficult to examine in such short windows of time [14]. In this project, small molecule drugs were delivered 24 hours prior to inducing injury via controlled cortical impact (CCI). In order to achieve clinical relevance, treatment via drug-loaded hydrogels post-injury should also be examined. Furthermore, drugs should be administered at a later time point (greater than 8 hours) following injury [14]. Results from pre- and post-injury treatment are expected to show similar decreases in cell death via PI cell counts. Another component of animal injury models that should be addressed to improve clinical relevance is the extent of injury. Examining the effect of drugs on a range of injury severities is crucial as TBI is highly heterogeneous in severity. Fortunately, an advantage of the CCI model is the control over the duration and depth of the impact onto the dura. Results are expected to indicate that higher doses of drug are required for higher impacts regardless of if injury was induced post- or pre-treatment. Again, the number of injured cells via PI counts should be used to quantify the therapeutic effect in each condition.

#### **6.1.4 Determine effect of large molecule drug delivery**

In this project, localized drug delivery to the brain was applied to the treatment of TBI. However, localized neural drug delivery has the potential for other applications such as the treatment of neurodegenerative diseases and the optimization of cancer therapy. Many of these additional applications require the delivery of large molecules (MW > 1000 Daltons). Thus, the last objective in the continuation of this project is to determine the effect of large molecule drug delivery. Albumin (Life Technologies, Grand Island, NY, USA) was also tested as a cell death marker in addition to PI where albumin was expected to mark larger injured cells with green fluorescence. Preliminary fluorescence results from the in vitro release of albumin (MW = 45 kDa, excitation = 494nm) from thin silk films into 1X PBS suggests that large molecules, such as proteins, release from silk. However, in vivo release displayed no green fluorescence at the predetermined dose. Results are expected to display successful delivery by increasing the dose. Additionally, the in vitro release of albumin from silk-HRP hydrogels should be examined before proceeding with in vivo hydrogel release. The aforementioned quantification methods for in vitro and in vivo release should be performed before loading large molecule drugs into the hydrogels. It is expected that hydrogels at a higher dose will also release albumin displaying green fluorescence in large injured cells. Further large molecule drug release should be screened and quantified in vitro before being loaded into silk-HRP hydrogels. While detection methods will vary among compounds, they are expected to have no interaction with silk. Once loaded into hydrogels, in vivo

release should be quantified with both PI and albumin markers. The effects of pre- and post-injury delivery should be observed as described in the previous aim. Results from large molecule drug release are expected to show a decrease in the number of cells marked with PI and albumin regardless of post- or pre-treatment.

## Bibliography

- [1] “CDC’s Report to Congress on Traumatic Brain Injury Epidemiology and Rehabilitation.” National Center for Injury Prevention and Control, 27-Mar-2015.
- [2] M. Faul and V. Coronado, “Epidemiology of traumatic brain injury,” *Handb. Clin. Neurol.*, vol. 127, pp. 3–13, 2015.
- [3] J. Dinsmore, “Traumatic brain injury: an evidence-based review of management,” *Contin. Educ. Anaesth. Crit. Care Pain*, p. mkt010, Feb. 2013.
- [4] R. C. Gardner and K. Yaffe, “Epidemiology of mild traumatic brain injury and neurodegenerative disease,” *Mol. Cell. Neurosci.*, Mar. 2015.
- [5] M. H. Sundman, E. E. Hall, and N.-K. Chen, “Examining the relationship between head trauma and neurodegenerative disease: A review of epidemiology, pathology and neuroimaging techniques,” *J. Alzheimers Dis. Park.*, vol. 4, Jan. 2014.
- [6] A. Tateno, T. Sakayori, Y. Takizawa, K. Yamamoto, K. Minagawa, and Y. Okubo, “A case of Alzheimer’s disease following mild traumatic brain injury,” *Gen. Hosp. Psychiatry*, vol. 37, no. 1, pp. 97.e7–9, Feb. 2015.
- [7] R. C. Gardner, J. F. Burke, J. Nettiksimmons, S. Goldman, C. M. Tanner, and K. Yaffe, “Traumatic brain injury in later life increases risk for Parkinson disease,” *Ann. Neurol.*, Feb. 2015.
- [8] P. Hamer, J. McGeachie, M. Davies, and M. Grounds, “Evans Blue Dye as an in vivo marker of myofibre damage: optimising parameters for detecting initial myofibre membrane permeability,” *J. Anat.*, vol. 200, no. 1, pp. 69–79, Jan. 2002.
- [9] P. Bahmani, E. Schellenberger, J. Klohs, J. Steinbrink, R. Cordell, M. Zille, J. Müller, D. Harhausen, L. Hofstra, C. Reutelingsperger, T. D. Farr, U. Dirnagl, and A. Wunder, “Visualization of cell death in mice with focal cerebral ischemia using fluorescent annexin A5, propidium iodide, and TUNEL staining,” *J. Cereb. Blood Flow Metab.*, vol. 31, no. 5, pp. 1311–1320, May 2011.
- [10] E. Esposito, I. Paterniti, E. Mazzon, T. Genovese, M. Galuppo, R. Meli, P. Bramanti, and S. Cuzzocrea, “MK801 attenuates secondary injury in a

- mouse experimental compression model of spinal cord trauma,” *BMC Neurosci.*, vol. 12, p. 31, Apr. 2011.
- [11] E. D. Hall, R. A. Vaishnav, and A. G. Mustafa, “ANTIOXIDANT THERAPIES FOR TRAUMATIC BRAIN INJURY,” *Neurother. J. Am. Soc. Exp. Neurother.*, vol. 7, no. 1, p. 51, Jan. 2010.
  - [12] J. Ghajar, “Traumatic brain injury,” *The Lancet*, vol. 356, no. 9233, pp. 923–929, Sep. 2000.
  - [13] “Traumatic Brain Injury: Hope Through Research,” *National Institute for Neurological Disorders and Stroke*, 22-Jul-2014. [Online]. Available: [http://www.ninds.nih.gov/disorders/tbi/detail\\_tbi.htm#266653218](http://www.ninds.nih.gov/disorders/tbi/detail_tbi.htm#266653218).
  - [14] D. J. Loane and A. I. Faden, “Neuroprotection for traumatic brain injury: translational challenges and emerging therapeutic strategies,” *Trends Pharmacol. Sci.*, vol. 31, no. 12, pp. 596–604, Dec. 2010.
  - [15] T. K. McIntosh, “Novel pharmacologic therapies in the treatment of experimental traumatic brain injury: a review,” *J. Neurotrauma*, vol. 10, no. 3, pp. 215–261, 1993.
  - [16] S. V. Kabadi and A. I. Faden, “Neuroprotective strategies for traumatic brain injury: improving clinical translation,” *Int. J. Mol. Sci.*, vol. 15, no. 1, pp. 1216–1236, 2014.
  - [17] W. Heegaard and M. Biros, “Traumatic Brain Injury,” *Emerg. Med. Clin. North Am.*, vol. 25, no. 3, pp. 655–678, Aug. 2007.
  - [18] Kushner D, “Mild traumatic brain injury: Toward understanding manifestations and treatment,” *Arch. Intern. Med.*, vol. 158, no. 15, pp. 1617–1624, Aug. 1998.
  - [19] S. M. Yamada, Y. Takaoka, and H. Matsuura, “A case of contrecoup skull fracture caused by mild head injury,” *Clin. Neurol. Neurosurg.*, vol. 125, pp. 106–108, Oct. 2014.
  - [20] “NINDS Shaken Baby Syndrome Information Page,” *National Institute of Neurological Disorders and Stroke*, 14-Feb-2014. [Online]. Available: <http://www.ninds.nih.gov/disorders/shakenbaby/shakenbaby.htm>.
  - [21] D. Shlosberg, M. Benifla, D. Kaufer, and A. Friedman, “Blood-brain barrier breakdown as a therapeutic target in traumatic brain injury,” *Nat. Rev. Neurol.*, vol. 6, no. 7, pp. 393–403, Jul. 2010.

- [22] M. Prins, T. Greco, D. Alexander, and C. C. Giza, "The pathophysiology of traumatic brain injury at a glance," *Dis. Model. Mech.*, vol. 6, no. 6, pp. 1307–1315, Nov. 2013.
- [23] K. Beauchamp, H. Mutlak, W. R. Smith, E. Shohami, and P. F. Stahel, "Pharmacology of traumatic brain injury: where is the 'golden bullet'?", *Mol. Med. Camb. Mass*, vol. 14, no. 11–12, pp. 731–740, Dec. 2008.
- [24] D. R. Lynch and T. M. Dawson, "Secondary mechanisms in neuronal trauma," *Curr. Opin. Neurol.*, vol. 7, no. 6, pp. 510–516, Dec. 1994.
- [25] X. Zhang, Y. Chen, L. W. Jenkins, P. M. Kochanek, and R. S. B. Clark, "Bench-to-bedside review: Apoptosis/programmed cell death triggered by traumatic brain injury," *Crit. Care Lond. Engl.*, vol. 9, no. 1, pp. 66–75, Feb. 2005.
- [26] A. Kumar and D. J. Loane, "Neuroinflammation after traumatic brain injury: Opportunities for therapeutic intervention," *Brain. Behav. Immun.*, vol. 26, no. 8, pp. 1191–1201, Nov. 2012.
- [27] J. V. Hunter, E. A. Wilde, K. A. Tong, and B. A. Holshouser, "Emerging imaging tools for use with traumatic brain injury research," *J. Neurotrauma*, vol. 29, no. 4, pp. 654–671, Mar. 2012.
- [28] B. L. Edlow and O. Wu, "Advanced neuroimaging in traumatic brain injury," *Semin. Neurol.*, vol. 32, no. 4, pp. 374–400, Sep. 2012.
- [29] A. I. Maas, N. Stocchetti, and R. Bullock, "Moderate and severe traumatic brain injury in adults," *Lancet Neurol.*, vol. 7, no. 8, pp. 728–741, Aug. 2008.
- [30] Y. Xiong, A. Mahmood, and M. Chopp, "Emerging treatments for traumatic brain injury," *Expert Opin. Emerg. Drugs*, vol. 14, no. 1, pp. 67–84, Mar. 2009.
- [31] M. M. Patel, S. V. Bfiadada, and A. F. Amin, "Getting into the Brain," pp. 35–59, 2009.
- [32] M. I. Alam, S. Beg, A. Samad, S. Baboota, K. Kohli, J. Ali, A. Ahuja, and M. Akbar, "Strategy for effective brain drug delivery.," *Eur. J. Pharm. Sci. Off. J. Eur. Fed. Pharm. Sci.*, vol. 40, no. 5, pp. 385–403, Aug. 2010.
- [33] E. H. Lo, A. B. Singhal, V. P. Torchilin, and N. J. Abbott, "Drug delivery to damaged brain," *Brain Res. Rev.*, vol. 38, no. 1–2, pp. 140–148, Dec. 2001.

- [34] R. Gabathuler, "Approaches to transport therapeutic drugs across the blood-brain barrier to treat brain diseases.," *Neurobiol. Dis.*, vol. 37, no. 1, pp. 48–57, Jan. 2010.
- [35] A. Misra, S. Ganesh, A. Shahiwala, and S. P. Shah, "Drug delivery to the central nervous system: a review," *J. Pharm. Pharm. Sci. Publ. Can. Soc. Pharm. Sci. Société Can. Sci. Pharm.*, vol. 6, no. 2, pp. 252–273, Aug. 2003.
- [36] S. C. Thal and W. Neuhaus, "The Blood-Brain Barrier as a Target in Traumatic Brain Injury Treatment," *Arch. Med. Res.*, Nov. 2014.
- [37] Y. Xiong, A. Mahmood, and M. Chopp, "Neurorestorative treatments for traumatic brain injury," *Discov. Med.*, vol. 10, no. 54, pp. 434–442, Nov. 2010.
- [38] A. I. Faden and S. Salzman, "Pharmacological strategies in CNS trauma," *Trends Pharmacol. Sci.*, vol. 13, pp. 29–35, 1992.
- [39] D. R. Namjoshi, C. Good, W. H. Cheng, W. Panenka, D. Richards, P. A. Crompton, and C. L. Wellington, "Towards clinical management of traumatic brain injury: a review of models and mechanisms from a biomechanical perspective," *Dis. Model. Mech.*, vol. 6, no. 6, pp. 1325–1338, Nov. 2013.
- [40] N. Marklund and L. Hillered, "Animal modelling of traumatic brain injury in preclinical drug development: where do we go from here?," *Br. J. Pharmacol.*, vol. 164, no. 4, pp. 1207–1229, Oct. 2011.
- [41] Y. Xiong, A. Mahmood, and M. Chopp, "Animal models of traumatic brain injury," *Nat. Rev. Neurosci.*, vol. 14, no. 2, pp. 128–142, Feb. 2013.
- [42] M. Zilberman and J. J. Elsner, "Antibiotic-eluting medical devices for various applications," *J. Control. Release Off. J. Control. Release Soc.*, vol. 130, no. 3, pp. 202–215, Sep. 2008.
- [43] E. M. Pritchard, T. Valentin, D. Boison, and D. L. Kaplan, "Incorporation of proteinase inhibitors into silk-based delivery devices for enhanced control of degradation and drug release," *Biomaterials*, vol. 32, no. 3, pp. 909–918, Jan. 2011.
- [44] Z. Ruszczak and W. Friess, "Collagen as a carrier for on-site delivery of antibacterial drugs," *Adv. Drug Deliv. Rev.*, vol. 55, no. 12, pp. 1679–1698, Nov. 2003.

- [45] E. M. Pritchard, T. Valentin, B. Panilaitis, F. Omenetto, and D. L. Kaplan, "Antibiotic-Releasing Silk Biomaterials for Infection Prevention and Treatment," *Adv. Funct. Mater.*, vol. 23, no. 7, pp. 854–861, Feb. 2013.
- [46] K. Numata and D. L. Kaplan, "Silk-based delivery systems of bioactive molecules," *Adv. Drug Deliv. Rev.*, vol. 62, no. 15, pp. 1497–1508, Dec. 2010.
- [47] H. Zhang, L. Li, F. Dai, H. Zhang, B. Ni, W. Zhou, X. Yang, and Y. Wu, "Preparation and characterization of silk fibroin as a biomaterial with potential for drug delivery," *J. Transl. Med.*, vol. 10, p. 117, 2012.
- [48] E. M. Pritchard and D. L. Kaplan, "Silk fibroin biomaterials for controlled release drug delivery," *Expert Opin. Drug Deliv.*, vol. 8, no. 6, pp. 797–811, Jun. 2011.
- [49] D. J. Hines and D. L. Kaplan, "Mechanisms of controlled release from silk fibroin films," *Biomacromolecules*, vol. 12, no. 3, pp. 804–812, Mar. 2011.
- [50] M. D. Tang-Schomer, X. Hu, M. Tupaj, L. W. Tien, M. Whalen, F. Omenetto, and D. L. Kaplan, "Film-based Implants for Supporting Neuron-Electrode Integrated Interfaces for The Brain," *Adv. Funct. Mater.*, vol. 24, no. 13, pp. 1938–1948, Apr. 2014.
- [51] N. Guziewicz, A. Best, B. Perez-Ramirez, and D. L. Kaplan, "Lyophilized silk fibroin hydrogels for the sustained local delivery of therapeutic monoclonal antibodies," *Biomaterials*, vol. 32, no. 10, pp. 2642–2650, Apr. 2011.
- [52] B. P. Partlow, C. W. Hanna, J. Rnjak-Kovacina, J. E. Moreau, M. B. Applegate, K. A. Burke, B. Marelli, A. N. Mitropoulos, F. G. Omenetto, and D. L. Kaplan, "Highly Tunable Elastomeric Silk Biomaterials," *Adv. Funct. Mater.*, vol. 24, no. 29, pp. 4615–4624, Aug. 2014.
- [53] D. Sierra-Mercado, L. M. McAllister, C. C. H. Lee, M. R. Milad, E. N. Eskandar, and M. J. Whalen, "Controlled cortical impact before or after fear conditioning does not affect fear extinction in mice," *Brain Res.*, Feb. 2015.
- [54] D. J. Hines and D. L. Kaplan, "Characterization of Small Molecule Controlled Release From Silk Films," *Macromol. Chem. Phys.*, vol. 214, no. 2, pp. 280–294, Jan. 2013.
- [55] Q. Lu, X. Hu, X. Wang, J. A. Kluge, S. Lu, P. Cebe, and D. L. Kaplan, "Water-Insoluble Silk Films with Silk I Structure," *Acta Biomater.*, vol. 6, no. 4, pp. 1380–1387, Apr. 2010.



- [56] X. Hu, K. Shmelev, L. Sun, E.-S. Gil, S.-H. Park, P. Cebe, and D. L. Kaplan, "Regulation of Silk Material Structure by Temperature-Controlled Water Vapor Annealing," *Biomacromolecules*, vol. 12, no. 5, pp. 1686–1696, May 2011.
- [57] A. M. Hopkins, L. De Laporte, F. Tortelli, E. Spedden, C. Staii, T. J. Atherton, J. A. Hubbell, and D. L. Kaplan, "Silk Hydrogels as Soft Substrates for Neural Tissue Engineering," *Adv. Funct. Mater.*, vol. 23, no. 41, pp. 5140–5149, Nov. 2013.
- [58] I. J. Reynolds, "[3H](+)MK801 radioligand binding assay at the N-methyl-D-aspartate receptor," *Curr. Protoc. Pharmacol. Editor. Board SJ Enna Ed.-Chief AI*, vol. Chapter 1, p. Unit 1.20, May 2001.